Hindawi
Geofluids
Volume 2023, Article ID 6236986, 21 pages
https://doi.org/10.1155/2023/6236986

Research Article

Study on Anisotropic Petrophysical Modeling of Shale: A Case Study of Shale Oil in Qingshankou Formation in Sanzhao Sag, Songliao Basin, China

Ang Li,[1,2] Liyan Zhang,[1] Jianguo Yang,[2] Shichao Li,[2] Fei Xiao,[2] Yulai Yao,[2] Yiming Huang,[2] Bo Liu,[3] and Longsheng Li[4]

[1]*China University of Petroleum-Beijing at Karamay, Karamay 834000, China*
[2]*Shenyang Centre of Geological Survey, China Geological Survey, Shenyang 110000, China*
[3]*Institute of Unconventional Oil & Gas, Northeast Petroleum University, Daqing 163318, China*
[4]*iRock Technologies Co., Ltd., Beijing 100094, China*

Correspondence should be addressed to Liyan Zhang; moonliyan@sohu.com

Received 11 September 2022; Revised 19 December 2022; Accepted 21 March 2023; Published 27 April 2023

Academic Editor: Jianchao Cai

Copyright © 2023 Ang Li et al. This is an open access article distributed under the Creative Commons Attribution License, which permits unrestricted use, distribution, and reproduction in any medium, provided the original work is properly cited.

Seismic petrophysics is an important link between seismic elastic properties and reservoir physical properties. Based on the petrological and microstructure characteristics of shale in the Qingshankou formation of Sanzhao sag in the north of Songliao Basin, this paper presents an anisotropy petrophysical model with complex pore structure suitable for organic shale constructed with the use of the Voigt-Reuss-Hill average model, an anisotropy self-consistent approximation+differential effective medium model, and the layering of clay and kerogen is simulated by using the Voigt-Reuss-Hill average and bond transform to achieve the simulation of shale anisotropy. Based on the proposed model, the effects of the organic volume fraction, porosity, and pore aspect ratio on rock elastic properties are discussed. The result shows that with the increase of matrix porosity, all elastic parameters show a decreasing trend; with the increase of the organic volume fraction, except shear modulus, other elastic parameters show an increasing trend. Through comparative analysis, the elastic parameters (Lamé impedance and Shear impedance) sensitive to the organic volume fraction and porosity are optimized; the seismic petrophysical cross-plot template with core calibration is constructed. The application shows that the predicted S-wave velocity based on the proposed model is in good agreement with the S-wave velocity derived from dipole source logging. Combined with the high-precision prestack elastic parameter inversion, the "sweet spot" characteristics can be well described, and the research could contribute to a better "sweet spot" description and provide a better support for shale exploration in Sanzhao sag.

1. Introduction

Shale oil and gas refers to resources remaining in place after primary and secondary oil and gas migration in the shale that has reached the oil generation threshold. The shale reservoir has the characteristics of large thickness, wide distribution range, low permeability, and good sealing, making it an important unconventional oil and gas reservoir resource and the most important continuous energy after conventional oil and gas resources [1–3]. As the shale oil and gas resources gradually play an important role in the energy pattern, it has become a hot research topic. In shale oil exploration and development, geological "sweet spot" evaluation and optimization are important foundations. The successful development of shale oil in the United States is due to the improvement of geological understanding and engineering technology progress, and the most important one is the ability to identify a "sweet spot" [4]. The "sweet spot" of shale oil refers to the reservoir intervals with more oil and better physical properties under the overall oil-bearing background. The geological demand of shale in these two aspects usually corresponds to the organic volume fraction and porosity. How to effectively evaluate these two parameters has become the key to the exploration and

development of shale oil [5]. At present, most of the prediction methods of the shale reservoir "sweet spot" are based on the elastic parameter volume (e.g., density) obtained by prestack elastic parameter inversion, and then the elastic parameter and "sweet spot" parameter are simply linearly fitted. This method has regional experience but lacks effective theoretical support. Therefore, many scholars try to establish a more accurate theoretical relationship between physical parameters and elastic parameters through accurate shale petrophysical modeling, so as to provide a reliable theoretical basis for the prediction of a shale oil reservoir "sweet spot."

Generally, shale has two types of minerals, one is rigid minerals (quartz, feldspar, calcite, pyrite, etc.), which are evenly distributed and have a stable particle size (aspect ratio), and the other is plastic minerals (clay), which are often fixed with kerogen and distributed in layers with strong anisotropy. In addition to layered minerals, flat pores are also the inducement of anisotropy. Therefore, how to effectively characterize the minerals, pores, and fluids in shale is an important content of shale rock physical modeling. In recent years, scholars have carried out a lot of research work on experimental and theoretical modeling in terms of shale anisotropic rock physical modeling and made some progress.

It is generally believed that shale anisotropy is mainly caused by two aspects. One is that the sedimentary stratification of clay and kerogen is the main contributing factor to VTI, and the other is that there are a large number of irregular pores and horizontal microfractures in shale, which will also enhance its anisotropy [6]. Laboratory studies have shown that the anisotropy of shale under dry conditions is determined by the preferred orientation of minerals and cracks parallel to stratification. Anisotropy tends to increase with the increase of the organic volume fraction, which leads to a decrease in density and thus an opposite effect to compaction. The assumption that shale has weak anisotropy cannot be used in shale seismic simulation [7, 8]. Generally, there are two kinds of effective medium theories in terms of shale anisotropy modeling, the average method and the SCA method [9–11]. Hornby et al. deduced the anisotropic SCA and DEM models based on the isotropic SCA and DEM models, the Gaussian distribution is used to simulate the directional arrangement distribution and stratification of clay and kerogen in shale and realize the anisotropic simulation [12]. Some scholars used the Backus average to simulate the mixture of layered clay and kerogen and obtained a good prediction except for C3s; the source of prediction error was determined as the layering of clay/kerogen, and an empirical parameter was introduced to make corrections [13, 14]. However, as the empirical fitting index seems to have no physical significance, the Backus average is not enough to simulate the kerogen, and only when the minerals are simple can the Backus average perform well [15, 16]. With the development of research, some scholars regard kerogen as the background medium, use the Voigt-Reuss-Hill (V-R-H) limit to calculate the equivalent elastic modulus of mixed rock minerals other than kerogen, and add the mixture to kerogen through the anisotropic DEM model to simulate the elastic properties of shale rich in organic matter [17, 18]. Some scholars also use anisotropic SCA and DEM models to simulate clay and fluid mixture, which was taken as background media; the equivalent elastic modulus of kerogen, quartz, calcite, and other mixtures is simulated by V-R-H, and finally, the anisotropic DEM model is used to add this mixture to the background medium [19, 20]. Some people presented that clay and kerogen mixture simulated by anisotropic SCA and DEM model is used as a background medium, the SCA model is used to simulate the brittle mineral mixture, and the anisotropic DEM is used to add the brittle mineral mixture to the background medium [21]. Some scholars presented that kerogen could be as the background medium, and SCA and DEM models are used to add pores to kerogen to ensure the interconnection between pores and kerogen. Finally, the Hashin-Shtrikman (H-S) limit model is used to calculate the equivalent elastic modulus of minerals other than kerogen and as an inclusion, and then DEM is used to add it to the background medium [22].

The shale oil in the north of Songliao basin in Northeastern China has high organic carbon content, moderate thermal evolution, large thickness, and wide distribution area. In recent years, large-scale volume fracturing technology has been adopted, and many wells have successively obtained industrial oil flow, revealing great resource potential and good exploration and development prospects. It has become an important replacement resource for the revitalization and development of Daqing Oilfield. Because the shale oil in the north of Songliao basin is different from the shale oil and gas in other basins at home and abroad in terms of origin, mineral type, organic matter type, and distribution form, there is no targeted petrophysical modeling theory at present, and its "sweet spot" geophysical response characteristics are not clear. Therefore, a seismic petrophysical model suitable for shale oil in this area is constructed and its petrophysical laws are analyzed, which are of great significance to establish an accurate petrophysical relationship between the "sweet spot" parameters and elastic parameters of shale. In this paper, the shale reservoir of Qingshankou formation (K_2qn) in Sanzhao sag in the northern part of the Songliao basin is considered as the research object. Firstly, the characteristics of shale mineral composition, organic matter distribution, and pore three-dimensional spatial distribution are systematically analyzed, and a seismic petrophysical model suitable for strong anisotropy of shale is constructed. The relationship between rock physical parameters and elastic parameters and the geophysical response characteristics of "sweet spot" is clarified. According to the petrophysical cross template of sensitive elastic parameters of organic matter volume fraction and porosity, combined with high-precision prestack elastic parameter inversion, the organic matter volume fraction and porosity are predicted, providing support for shale oil exploration deployment in Sanzhao depression.

2. Geological Information

Songliao basin is located in northeastern China. It is a large continental depression-type sedimentary basin dominated

by Mesozoic sediments. It is the continental sandstone-type petroliferous basin with the most abundant oil and gas resources in the world, with an area of about 26×10^4 km^2. The formation and evolution of the Songliao basin have roughly gone through four stages of thermal uplift dehiscence, rifting, depression, and shrinkage. The strata in the depression period are divided into six first-order structural units according to the development characteristics of regional uplift and depression, namely, the north dipping area, the central depression area, the northeastern uplift area, the southeast uplift area, the southwest uplift area, and the western slope area. The central depression area includes Heiyupao sag, Mingshui terrace, Longhupao-Honggang terrace, Qijiagulong sag, Daqing placanticline, Sanzhao sag, Chaoyanggou terrace, Changling sag, and Fuyu-Huazijing terrace (Figures 1(a) and 1(b)). Sanzhao sag is located in the northeastern central depression area in the north of the Songliao basin. It is a secondary negative structural unit in the central depression area of the Songliao basin. It was formed by the uplift of Daqing placanticline and Chaoyanggou terrace after the disintegration of the ancient central uplift. It is one of the most important oil-generating and oil-rich sags in the Songliao basin. The strata discovered in Sanzhao sag are mainly composed of Mesozoic and Cenozoic strata. From bottom to top, they are the Cretaceous Huoshiling formation, Shahezi formation, Yingcheng formation, Denglouku formation, Quantou formation, Qingshankou formation (K_2qn), Yaojia formation, Nenjiang formation, Sifangtai formation, Mingshui formation, and Paleogene Yian formation, Neogene and Quaternary sedimentary strata. Qingshankou formation (K_2qn) is the main hydrocarbon source rock series of Sanzhao sag; shale has a large development thickness (70-100 m), wide distribution range (favorable exploration area of 2969.95 km^2), high organic matter abundance, moderate maturity evolution, and huge shale oil resource potential. The study area is selected in the Xujiaweizi syncline in the middle of Sanzhao sag, which is the main part of Sanzhao sag (Figure 1(c)).

Qingshankou formation (K_2qn) is the main target layer for shale oil exploration in Sanzhao sag. Based on the selection and comparison of standard wells, according to the lithological combination, color, and electrical characteristics, combined with the index parameters such as paleosalinity, paleowater depth index, and biological fossils, the Qingshankou formation (K_2qn) is divided into two first-order sequence (XF1 and XF2), two second-order sequence (OSB1 and OSB2), and five third-order sequence (DSB1, DSB2, DSB3, DSB4, and DSB5). Among them, XF1 is the interface between Quantou formation with tight sandstone and Qingshankou formation (K_2qn) of rich organic shale. The interface is a sudden contact in lithology, forming obvious strong continuity seismic reflection at the interface. XF2 is the interface between the Qingshankou formation (K_2qn) and Yaojia formation (K_2y) with large delta facies sandstone, and the interface has obvious strong continuity seismic reflection. The interface of OSB1 corresponds to the top of the K_2qn_1 member. Above the interface is gray-black mudstone developed at the bottom of K_2qn_2 member. Below the interface is a set of 2-3 m ostracod containing silty mudstone. The seismic response is relatively continuous medium and weak amplitude. The interface of OSB2 corresponds to the top interface of K_2qn_2 member. Above the interface is gray-black mudstone developed at the bottom of K_2qn_3 member. Below the interface is a set of 2-3 m ostracod containing silty mudstone; the seismic response is characterized by weak amplitude and local blank reflection; DSB1, DSB2, DSB3, DSB4, and DSB5, respectively, correspond to the top interfaces of $K_2qn_1{}^3$, $K_2qn_1{}^2$, $K_2qn_2{}^2$, $K_2qn_3{}^3$ and $K_2qn_3{}^2$ submember (Figure 2.)

The "sweet spot" section of shale oil in the Qingshankou formation (K_2qn) is mainly concentrated in the first and second members of the Qingshankou formation (K_2qn). According to the statistics of geological parameters of the target layer, the rock color of Qingshankou formation (K_2qn) gradually becomes lighter from bottom to top, and gradually transits from gray-black to gray. The Th/U value gradually increases, reflecting that the water body gradually becomes lower. The Qingshankou formation (K_2qn) is a set of reverse cycle sedimentation, and the sedimentary environment is saline, freshwater, wet, and reducing environment.

The organic volume fraction gradually increases from top to bottom, with the highest reaching 7.99% in the $K_2qn_1{}^2$ submember. The GR, DT, CNL, and LLD all reveal a gradually increasing trend, and the DEN gradually decreases, reflecting the gradual development of shale, the gradual increase of porosity, and the improvement of oil-bearing property (Table 1).

3. Microstructure

3.1. Petrological Characteristics. Through X-ray diffraction of 269 shale core samples from Qingshankou formation (K_2qn) in Sanzhao sag, it can be seen that the mineral components of the rock matrix mainly include clay minerals, quartz, feldspar, calcite, and pyrite, and the mineral composition changes greatly in the vertical direction. From bottom to top, the quartz content changes from low to high, the clay content changes from low to high to low, the feldspar content changes from low to high, and the organic volume fraction changes from low to high. The average quartz content in K_2qn_1 is 33.92%, and the average quartz content in K_2qn_2 is 34.20%. The quartz content of the two members is basically the same; the average clay content in K_2qn_1 is 36.91%, and the average clay content in K_2qn_2 is 33.89%. The clay content in K_2qn_1 is slightly higher than that in K_2qn_2. The average feldspar content in K_2qn_1 is 20.38%, and the average feldspar content in K_2qn_2 is 22.73%. The feldspar content in K_2qn_2 is slightly higher than that in K_2qn_1. The calcite and pyrite content in the first and second members of the Qingshankou formation (K_2qn) is lower than 10%, and the content of the two minerals is basically the same. In K_2qn_1, the quartz content of $K_2qn_1{}^3$ is 35.71%, slightly higher than that of $K_2qn_1{}^2$ (32.82%) and $K_2qn_1{}^1$ (33.24%). The clay content gradually decreases from bottom to top. The clay content of $K_2qn_1{}^3$ is the highest (53.15%), followed by $K_2qn_1{}^2$ (40.28%), and $K_2qn_1{}^1$

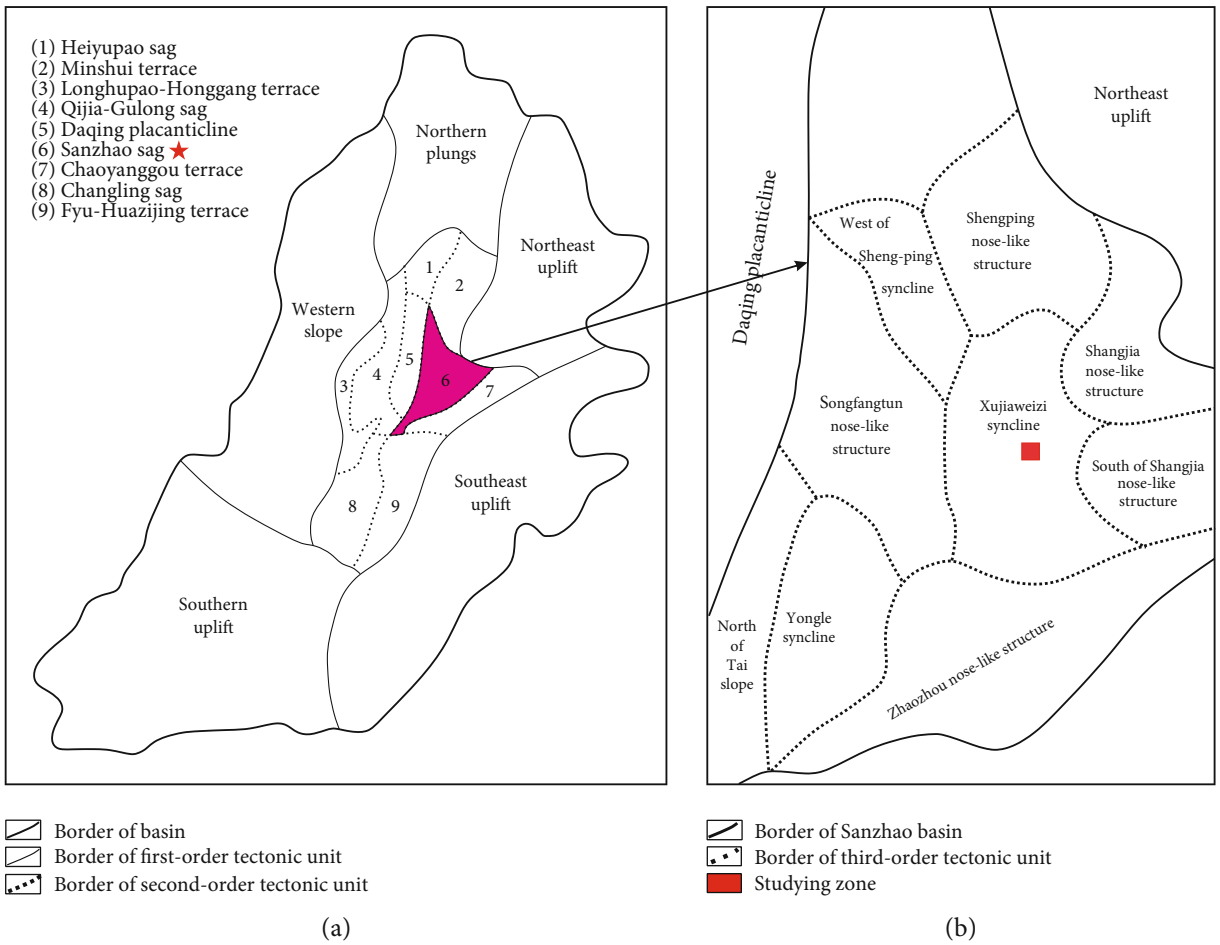

Figure 1: Structural location map of the study area. (a) Location map of Songliao Basin; (b) structural location map of Sanzhao sag.

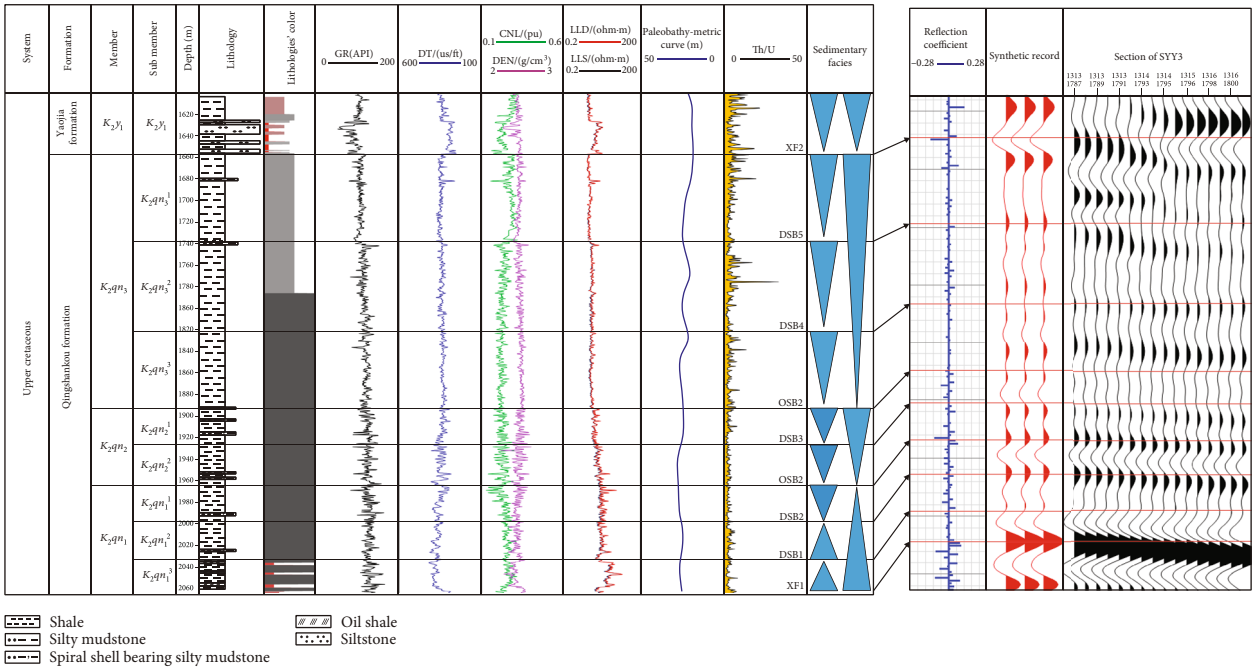

Figure 2: Comprehensive map of stratigraphic division, sedimentary facies, and seismic facies of well SYY3.

Table 1: Characteristics of Qingshankou formation (K_2qn).

Formation	Lithology	Color	TOC	GR (API)	P-acoustic time us/m	CNL (pu)	DEN (g/cm^3)	LLD (ohm.m)	TH_U	Paleobathymetric (m)	Paleosalinity	Ancient climate	Palaeoenvironment	Seismic reflection characteristics
$K_2qn_2^1$	Mudstone, shale, ostracod silty mudstone, ostracod containing mudstone	Gray black	0-4.26 1.46	88.60-151.89 125.10	289.17-378.96 336.98	0.17-0.29 0.22	2.37-2.58 2.47	2.37-5.78 3.46	0.76-8.03 0.22	25.0-26.0 25.5	Freshwater brackish water	Humid climate	Reduction environment	Weak peak, high continuity, local blank reflection
$K_2qn_2^2$	Mudstone, shale, silty mudstone with ostracod, ostracod bearing mudstone	Gray black	0-6.6 2.47	90.15-157.97 125.81	284.05-405.11 348.22	0.14-0.3 0.23	2.23-2.61 2.44	3.26-13.19 5.09	1-4.7 2.42	26.0-28.5 27.4				Medium weak peak, high continuity
$K_2qn_1^1$	Mudstone, shale, silty mudstone containing a small amount of ostracods, ostracod-bearing mudstone	Gray black	0.86-6.17 2.94	85.08-164.50 128.20	295.12-397.66 351.65	0.13-0.29 0.23	2.36-2.56 2.44	4.5-23.73 6.90	0.79-5.2 2.28	26.0-27.8 26.9				Medium strong peak, high continuity
$K_2qn_1^2$	Mudstone, shale, silty mudstone with a small amount of ostracod containing	Gray black	1.08-6.73 3.37	109.63-153.15 127.74	333.20-413.51 369.65	0.22-0.31 0.25	2.32-2.52 2.43	3.71-14.58 6.41	1.13-6.93 2.92	24.7-25.9 25.3				Medium strong peak, high continuity
$K_2qn_1^3$	Mudstone, shale and three sets of oil shale marker beds	Gray black、black brown	0-7.99 3.76	105.78-166.58 130.931	298.28-418.47 378.91	0.19-0.31 0.26	2.26-2.53 2.41	3.73-39.9 12.30	0.96-7.89 2.64	25.7-27.2 26.5	Saltwater			Weak peak, medium-low continuity

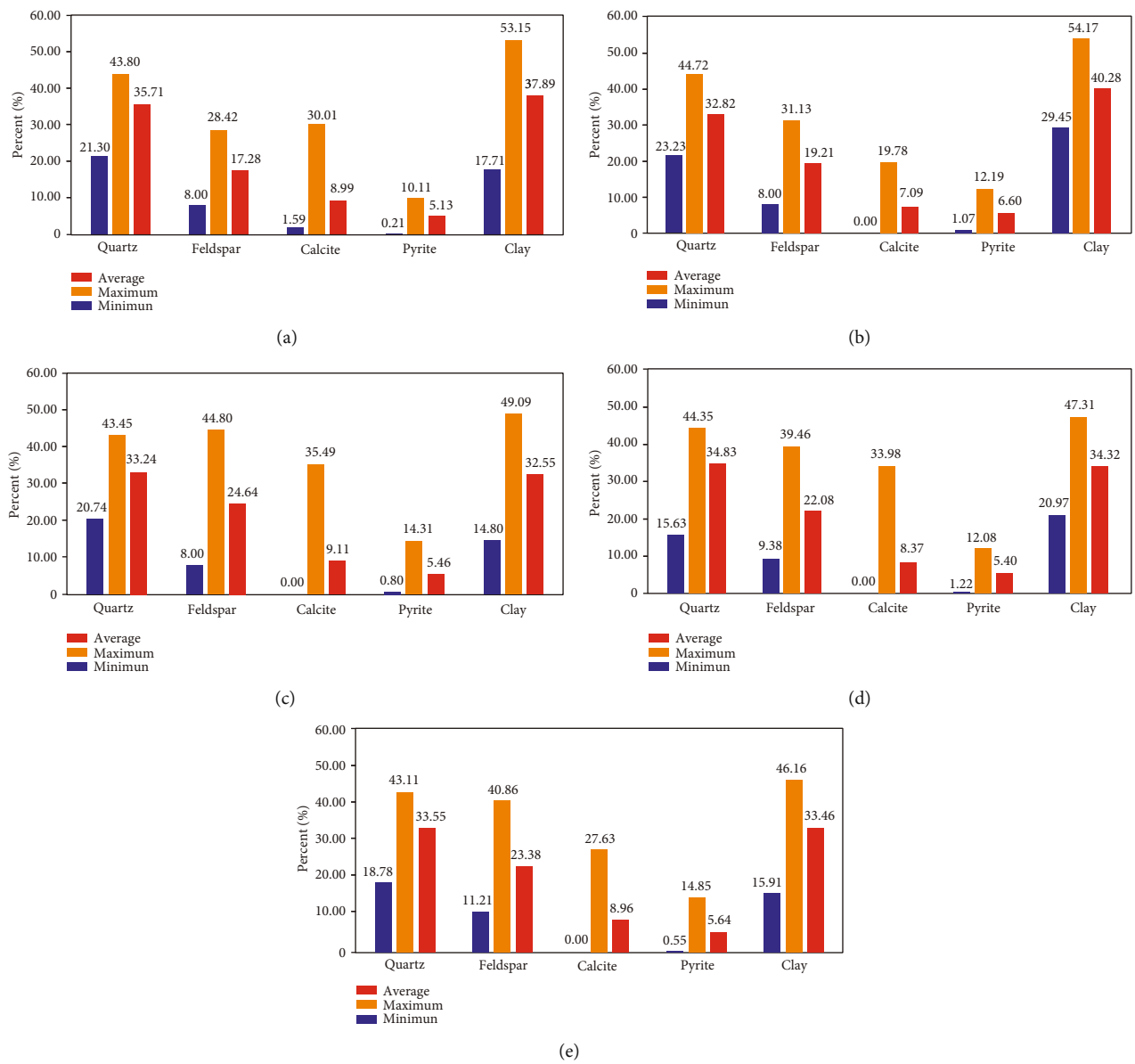

Figure 3: Mineral composition histogram of well SYY3. (a) Histogram of minerals composition of $K_2qn_1^3$, (b) histogram of minerals composition of $K_2qn_1^2$, (c) histogram of minerals composition of $K_2qn_1^1$, (d) histogram of minerals composition of $K_2qn_2^2$, and (e) histogram of minerals composition of $K_2qn_2^1$.

(32.55%). The clay content gradually increases from bottom to top. The feldspar content of $K_2qn_1^3$ is 17.28%, that of $K_2qn_1^2$ is 19.21%, and that of $K_2qn_1^1$ is 24.64% (Figure 3).

Compared with Gulong sag, Qijia sag of Songliao basin, Weiyuan area in Sichuan, China, and Barnett shale of Vosberg Basin, USA (Figure 4) [23–25], it is found that in the same basin, the content of quartz feldspar of Qingshankou formation (K_2qn) in Sanzhao sag is equal to that of Gulong sag, slightly higher than that of Qijia sag, and the content of carbonate is lower than that of Gulong sag and equal to that of Qijia sag. The content of clay in Sanzhao sag and Gulong sag is the same, so the contents of brittle minerals and clay minerals in the three major depressions of the Songliao basin are the same, with little difference. However, compared with the shale in the Weiyuan area of the Sichuan Basin and Barnett shale in the Vosberg Basin, the mixed layer clay in Sanzhao sag reveals an orderly characteristic, indicating that the shale of Qingshankou formation (K_2qn) has entered the late diagenetic stage. Brittle minerals are richer in Sanzhao sag, which belongs to the silicon-rich shale oil reservoir. The clay mineral content is relatively low, which also creates favorable conditions for later hydraulic fracturing. The brittle minerals in Barnett shale are mainly biogenic and diagenetic, while the brittle minerals in Sanzhao sag are mainly terrigenous quartz and feldspar.

3.2. Microstructure Characteristics. The rock structure of Qingshankou formation (K_2qn) shale is relatively complex. According to the observation results of scanning electron

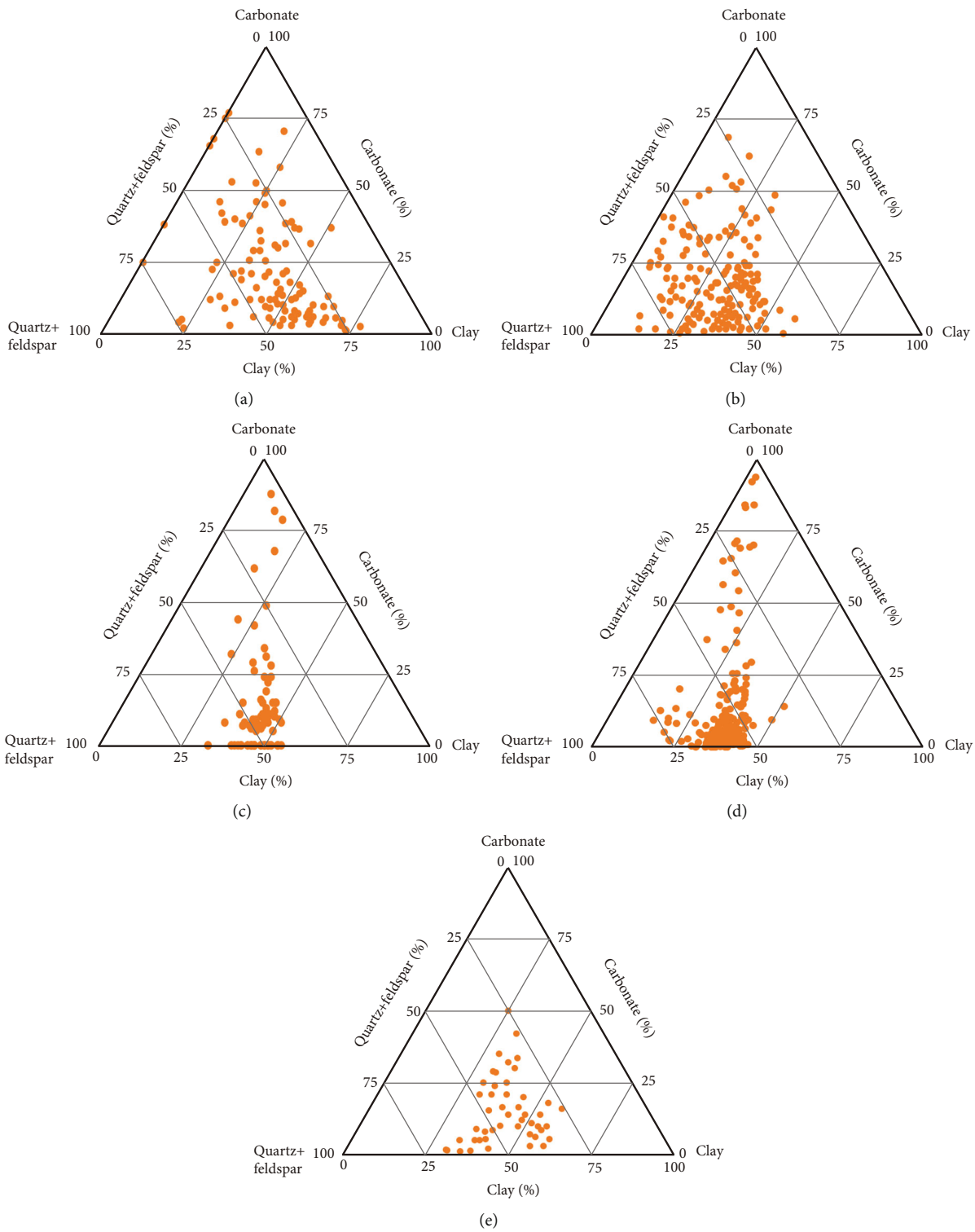

Figure 4: Comparison of minerals between Sanzhao sag and other basins. (a) Triangle chart of the mineral composition of Barnet sag in the USA, (b) triangle chart of the mineral composition of Gulong sag in China, (c) triangle chart of the mineral composition of Qijia sag in China, (d) triangle chart of the mineral composition of Sanzhao sag in China, and (e) triangle chart of the mineral composition of Weiyuan area of Sichuan sag in China.

microscope and backscatter electron microscope (Figure 5), the reservoir space of Qingshankou formation (K_2qn) can be divided into three types according to the genesis and geometric shape: micro and nanopores composed of an inorganic mineral matrix, organic nanopores, and fractures. There are two types of micro and nanopores composed of an inorganic mineral matrix: intergranular pores and intragranular pores. Intergranular pores can be divided into residual

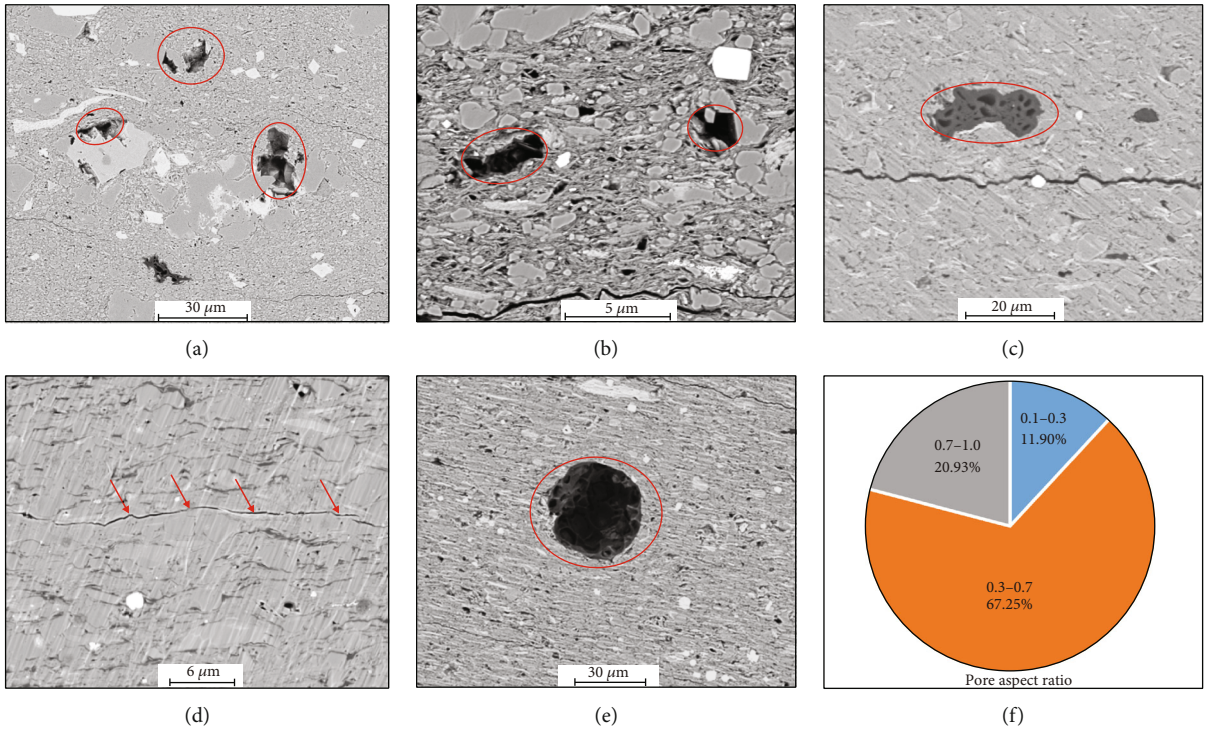

Figure 5: Pore types of Sanzhao sag. (a) Intergranular pores, (b) intergranular dissolved pores, (c) organic matter pores, (d) fractures, (e) dissolved pores, and (f) pore aspect ratio.

primary/dissolved intergranular pores, intergranular pores, rigid particle edge pores, and clay mineral intergranular pores, with a pore size of 4-40 μm. Intragranular pores include intragranular dissolved pores, intracrystalline pores, and clay mineral aggregate pores, with a pore size of 0.6-2 μm. The pore size of organic matter is 1-10 μm. The pore geometric characteristics are obtained by using digital lithological technology in four core samples of SYY3. The aspect ratio of pores is obtained from the scanned digital images (Figure 5(e)). It can be seen that the pore aspect ratio of Qingshankou Formation (K_2qn) is distributed in 0-1, mainly in 0.3-0.7, and the average value is about 0.55, which is used as the parameter for porosity modeling. Fractures include clay mineral interlayer fractures and microfractures. The porosity is high, with a distribution range of 3.5-9.8% and an average of 7.4%. The shale of Qingshankou formation (K_2qn) in Sanzhao sag has a large burial depth and high maturity. The vitrinite reflectance is 0.75-0.98%, with an average of 0.88%. The organic matter is in the main stage of hydrocarbon generation. Organic matter is the material basis for shale oil generation and the most important control factor for shale oil and gas enrichment. According to the observation of a scanning electron microscope (Figure 6), it can be seen that the organic matter of shale is mainly distributed between the rock matrix minerals and in the primary intergranular pores, in the form of strip and agglomerate, respectively. The strip organic matter is mainly developed between layered illite and deposited at the same time with illite. Organic matter can be used as a continuous matrix to support the rock and bear a certain force, which makes the rock have certain anisotropic characteristics. However, this anisotropy is slightly different from the organic matter of the immature Bakken shale in the United States. Almost all organic matter in the Bakken shale presents a strip distribution of approximately parallel bedding, which makes the shale have strong anisotropy.

The micropore structure of a reservoir refers to the geometry, size, distribution, and mutual connection of pores and throats in rocks. The micropore characteristics of rocks directly affect the reservoir and flowing capacity. In order to describe the micropore structure of rock samples more precisely, the air-cooled wire-cutting technology is applied to drill the samples with a diameter of 2.5 mm, and the three-dimensional digital core CT scanning method [26–30] is applied to conduct all-round and large-scale rapid nondestructive scanning imaging of rock samples, so as to vividly reveal the spatial characteristics of sample pore structure and mineral distribution. The digital core scanning results of shale samples obtained by CT detection include the pore throat ball-and-stick model and pore connectivity model. Figure 7 reveals the pore throat ball-and-stick model of the sample, with a size of 200 μm × 200 μm × 200 μm, the left figure is the 3D pore structure diagram of the pore throat ball-and-stick of massive felsic shale, and the right figure is the pore throat ball-and-stick model of laminated felsic shale. It can be seen from the figure that the pores of the massive shale samples are mostly isolated pores with poor connectivity. Compared with the massive shale samples, the pores of the laminar shale samples in the K_2qn_1 member have good connectivity. It can also be seen that part of the

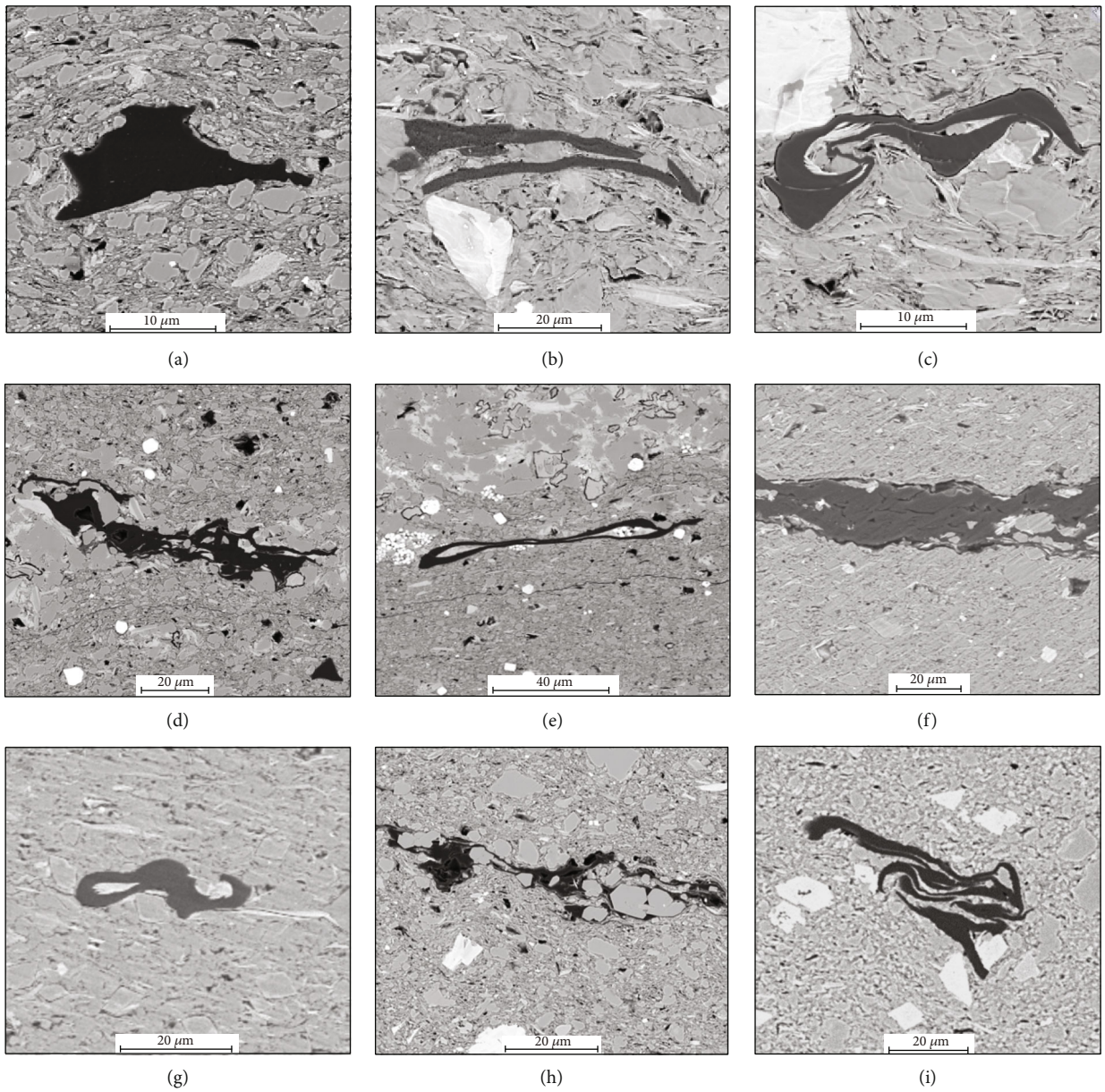

Figure 6: Distribution of organic matter. (a) Agglomerate organic matter, (b–i) strip organic matter.

interlayer fractures run through the samples. The pores are mainly coin-shaped and oblong ellipsoid, with a low pore aspect ratio.

4. Petrophysical Modeling for Shale

The seismic petrophysical theory is an important link between seismic elastic properties and reservoir physical properties. Compared with conventional sandstone, the strong anisotropy of shale makes the petrophysical modeling more difficult. Its genesis can be briefly summarized into two main aspects: (1) clay particles and kerogen in shale are usually distributed in layers, which lead to strong anisotropy; (2) shale has flat pores and transversely distributed micro-fractures, and complex pore and fracture structures will cause anisotropy as well. Through the above analysis of the basic geological characteristics of the shale of Qingshankou formation (K_2qn) in Sanzhao sag, it is found that the rock structure is relatively complex, the porosity aspect ratio is low, and the porosity with the aspect ratio of 0.1-0.7 accounts for more than 70% of the total pore type. In addition, a large number of horizontal bedding fractures are also developed, and the clay minerals and organic matter are regularly distributed in strips, which makes the shale in this area show strong anisotropy. In view of the special characteristics of shale oil deposition and diagenesis in Qingshankou formation (K_2qn) in the north of Songliao basin, in order to accurately describe the anisotropic properties of shale, an anisotropic seismic petrophysical model of shale with complex pore structure is constructed for Qingshankou formation (K_2qn) in Songliao basin. Firstly, a double-connected kerogen clay mixture is constructed by

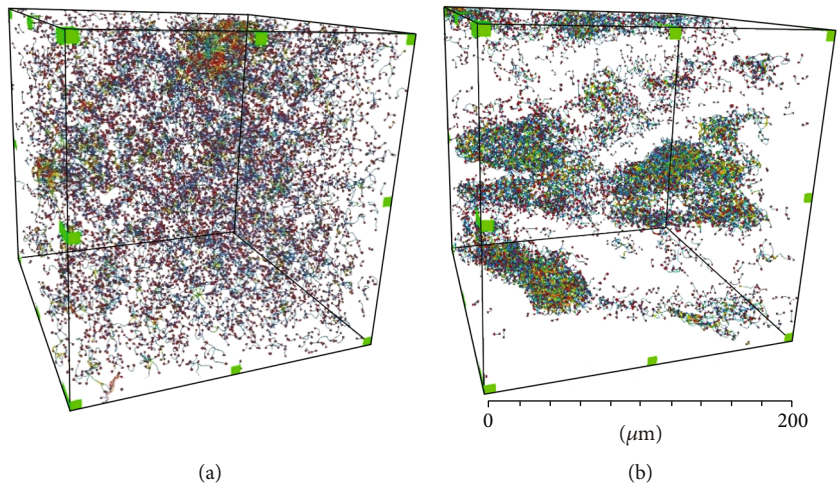

Figure 7: Micropore structure of shale of Qingshankou Formation in Sanzhao sag. (a) The 3D pore structure diagram of pore throat ball-and-stick of massive felsic shale and (b) the 3D pore structure diagram of pore throat ball-and-stick of laminated felsic shale.

using anisotropic SCA+DEM, and then the layering of clay and kerogen is simulated by using V-R-H average and bond transform to achieve the simulation of shale anisotropy. The process is shown in Figure 8.

4.1. Equivalent Elastic Modulus of Rock Matrix

4.1.1. Voigt-Reuss-Hill Average. V-R-H average [31] can be applied to calculate the equivalent elastic modulus of isotropic and completely elastic media. In the matrix components of mud-shale of Qingshankou formation (K_2qn) in Sanzhao sag, quartz, feldspar, calcite, and pyrite are all rigid media with similar elastic properties and can be mixed with this model.

The expression is as follows:

$$M_{\mathrm{VRH}} = \frac{M_{\mathrm{V}} + M_{\mathrm{R}}}{2}, \tag{1}$$

where

$$M_{\mathrm{V}} = \sum_{i=1}^{N} \varphi_i M_i, \frac{1}{M_R} = \sum_{i=1}^{N} \frac{\varphi_i}{M_i}, \tag{2}$$

where φ_i and M_i are the volume fraction and elastic modulus of the ith component, respectively; M_{VRH} is the elastic modulus of mixed minerals.

4.1.2. Anisotropy SCA Theory. Based on the KT model, Budiansky and Hill [32, 33] proposed the isotropic self-consistent approximation theory. The self-consistent approximation theory regards each mineral component and pore fluid as independent phases and considers the interaction between different phases. The self-consistent theory satisfies the high-frequency hypothesis, so the theory is generally in good agreement with the laboratory measurement results. In recent years, the SCA model has been widely applied in the construction of the shale model, mainly as the mineral components of shale are complex, and the SCA model can be equivalent to multiphase minerals at the same time, which provides convenience for the simulation of shale. However, when the fluid phase and solid phase are equivalent by using the SCA model, and the porosity exceeds 60%, the equivalent result of SCA will coincide with the lower limit of the Hashin-Shtrikman boundary. At this time, the rock is in a state of "particle suspension," that is, the pore fluid phase completely surrounds the solid phase. At this time, the solid particles do not communicate with each other. Therefore, when the porosity is 40%-60%, the two-phase materials can keep connecting with each other. The model considers the interaction of inclusions close to each other and is applicable to the case that a variety of minerals act as the rock matrix. Different mixed minerals have the same content, without absolute dominant components. The self-consistent model is most suitable. The model expression is as follows:

$$\sum_{i=1}^{N} \varphi_i (K_i - K_{SC}^*) P^{*i} = 0, \tag{3}$$

$$\sum_{i=1}^{N} \varphi_i (\mu_i - \mu_{SC}^*) Q^{*i} = 0, \tag{4}$$

where K_{SC}^*, μ_{SC}^* are the bulk modulus and shear modulus of the equivalent medium obtained by the model; i is the ith component, φ_i, K_i, μ_i is its volume fraction, bulk modulus, and shear modulus, respectively; P^{*i} and Q^{*i} are coefficients related to inclusion i.

As stated in the above introduction part, based on the isotropic inclusion theory, Hornby extended the SCA model to the anisotropic form, and the isotropic parameter bulk modulus (K) and shear modulus (μ) in the original formula are replaced by tensor matrix C. The factors (P, Q)

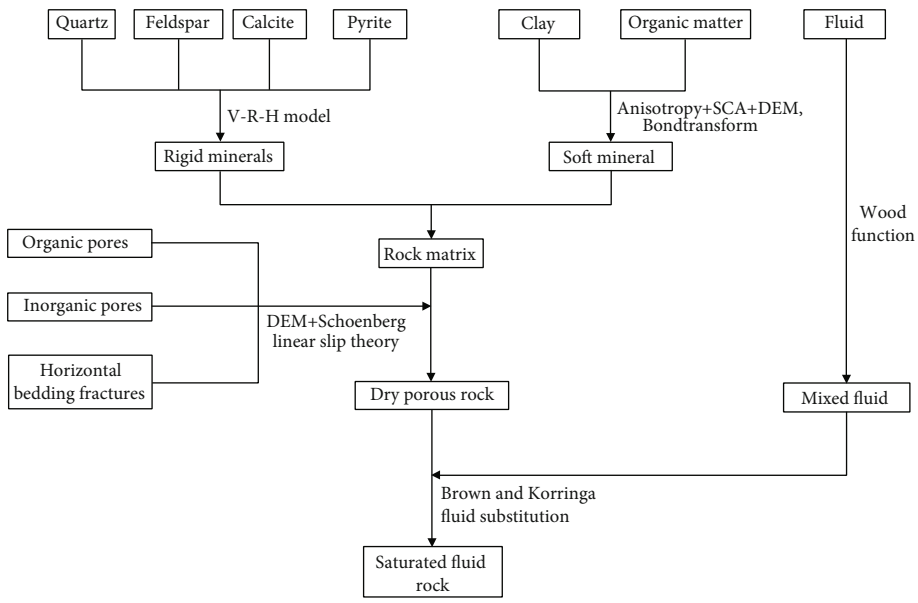

Figure 8: Anisotropy petrophysical modelling process of shale.

controlling the shape of inclusions are replaced by tensor matrix G. The formula is as follows:

$$\begin{aligned}\tilde{C}_{ck_05} = &\left\{0.5\tilde{C}_c\left[\tilde{I}_{ijkl} + \tilde{G}^c_{ijkl}\left(\tilde{C}_c - \tilde{C}_{ck_{05}}\right)\right]^{-1}\right.\\ &\left.+0.5\tilde{C}_k\left[\tilde{I}_{ijkl} + \tilde{G}^k_{ijkl}\left(\tilde{C}_k - \tilde{C}_{ck_{05}}\right)\right]^{-1}\right\}\\ &\bullet\left\{0.5\tilde{I}_{ijkl}\left[\tilde{I}_{ijkl} + \tilde{G}^c_{ijkl}\left(\tilde{C}_c - \tilde{C}_{ck_{05}}\right)\right]^{-1}\right.\\ &\left.+0.5\tilde{I}_{ijkl}\left[\tilde{I}_{ijkl} + \tilde{G}^k_{ijkl}\left(\tilde{C}_k - \tilde{C}_{ck_{05}}\right)\right]^{-1}\right\}^{-1},\end{aligned} \tag{5}$$

where $\tilde{C}_{ck_05}$ is the equivalent stiffness tensor of 50% clay and 50% kerogen, GPa; $\tilde{C}_c$ and $\tilde{C}_k$ are the stiffness tensor of clay and kerogen, GPa; $\tilde{I}_{ijkl}$ is a fourth-order unit tensor, dimensionless; $\tilde{G}^c_{ijkl}$ and $\tilde{G}^k_{ijkl}$ are the Eshelby tensor of clay and kerogen, respectively, dimensionless. The Eshelby tensor is calculated by the following formula:

$$\hat{G}_{ijkl} = \frac{1}{8\pi}\left(\bar{G}_{ijkl} + \bar{G}_{jkil}\right), \tag{6}$$

where $\hat{G}_{ijkl}$ is related to the aspect ratio of inclusions.

4.1.3. Anisotropy DEM Theory. The differential effective medium (DEM) model simulates the two-phase mixture by gradually adding filler to the solid phase [34, 35]. The solid mineral is the material of phase 1, and then phase 2 is added gradually. This process continues until the required content of each component is reached. DEM theory does not treat each component symmetrically. The components considered as solid minerals or main phases can be selected differently, and the final equivalent modulus will depend on the path to the final mixture. Using phase 1 as the main phase and gradually adding material 2, or using phase 2 as the main phase and gradually adding material 1, will lead to different equivalent properties. The formula can be expressed as follows:

$$(1-y)\frac{d}{dy}\left[K^*_{dry}(y)\right] = (K_2 - K^*_{SCA})P^{(*2)}(y), \tag{7}$$

$$(1-y)\frac{d}{dy}\left[\mu^*_{dry}(y)\right] = (\mu_2 - \mu^*_{SCA})Q^{(*2)}(y), \tag{8}$$

where K^*_{dry}, μ^*_{dry} represents the bulk modulus and shear modulus of dry rock, respectively; K^*_{dry}, μ^*_{dry}, respectively, represent the bulk modulus and shear modulus of dry rock under critical porosity; when $\rho > \rho_c$ (critical porosity), K_2, μ_2 represents the bulk modulus and shear modulus of phase 2 (pore phase), respectively, and y represents the percentage of phase 2, that is, the true porosity φ; when $\rho < \rho_c$ (critical porosity), K_2, μ_2 represents the bulk modulus and shear modulus of phase 1 (matrix phase), respectively, and y represents the percentage of phase 1.

Similarly, Hornby extended the DEM model to the anisotropic form as well, the isotropic parameter bulk modulus (K)and shear modulus (μ) in the original formula are replaced by tensor matrix C. The factors (P,Q) controlling the shape of inclusions are replaced by tensor matrix G. The formula is as follows:

$$\begin{aligned}\frac{d}{dy}\left[\tilde{C}_{ck}(v_{rc})\right] = &\frac{1}{1-v_{rc}}\left[\tilde{C}_c - \tilde{C}_{ck}(v_{rc})\right]\\ &\bullet\left\{\tilde{I}_{ijkl} + \tilde{G}_c\left[\tilde{C}_c - \tilde{C}_{ck}(v_{rc})\right]\right\}^{-1},\end{aligned} \tag{9}$$

where v_{rc} is the relative content of residual clay to be added to the background, and it meets the following: $v_{rc} = 2v_c - 1$, dimensionless; v_c is the true content of clay, dimensionless;

$\tilde{C}_{ck}$ is the equivalent stiffness tensor of clay and kerogen mixture, GPa; $\tilde{C}_c$ is the stiffness tensor of clay, GPa; $\tilde{G}_c$ is the Eshelby stiffness tensor of clay, dimensionless; $\tilde{I}_{ijkl}$ is the fourth-order unit stiffness tensor, dimensionless. The equation can be solved by using the fourth-order Runge-Kutta method [36], and the initial value in the iterative solution process meets the following: $\tilde{C}_{ck}(\nu_{rc} = 0) = \tilde{C}_{ck_05}$.

4.1.4. Anisotropy Simulation of Clay and Kerogen. Petrophysical modeling needs the volume fraction of each mineral (including organic matter). Generally, the volume fraction of inorganic minerals (quartz, feldspar, calcite, dolomite, clay, etc.) can be obtained through X-ray diffraction, the total organic carbon (TOC) is obtained by combustion, which is a weight fraction. Therefore, it is necessary to make a conversion from the weight fraction to the volume fraction of organic matter. The conversion formula is as follows:

$$\rho_1 = \sum_{i=1}^{n} V_{\theta i} * \rho_i, \tag{10}$$

$$V_1 = \frac{W_{\theta 1}/\rho_1}{((W_{\theta 1}/\rho_1) + (1 - W_{\theta 1}/\rho_2))}, \tag{11}$$

$$V_2 = \frac{1 - W_{\theta 1}/\rho_2}{((W_{\theta 1}/\rho_1) + (1 - W_{\theta 1}/\rho_2))}, \tag{12}$$

where ρ_1 and ρ_2 are the equivalent density of inorganic minerals and the density of organic matter, respectively, ρ_i and $V_{\theta i}$ are the density and the volume fraction of each inorganic mineral; V_1, V_2, $W_{\theta 1}$, and $W_{\theta 2}$ are the volume fraction and weight fraction of inorganic minerals and organic matter, respectively. In order to simulate the layering of clay and kerogen and then realize the anisotropic simulation of shale, firstly, anisotropic SCA+DEM is applied to mix isotropic clay and kerogen to obtain kerogen clay blocks with interconnected properties; the layering of shale is simulated by rotating and stacking many identical clay kerogen blocks. The elastic properties of the clay blocks after rotation can be calculated by bond transformation, and the Voigt Reuss Hill average can be applied to calculate the equivalent properties of clay block stacking at different angles. The equivalent modulus of other brittle minerals except clay and kerogen are calculated by Voigt-Reuss-Hill average. Finally, the equivalent material composed of layered clay kerogen blocks is used as the background, and the anisotropic DEM model is applied to add the isotropic brittle mixture and pores into the background medium to obtain the final equivalent result.

4.2. Elastic Modulus of Complex "Dry" Pore Rock. By using DEM theory, the randomly distributed coin-like pores with a single aspect ratio are added to the rock matrix to obtain the initial "dry" pore rock. On this basis, the dry fractures are added to the rock matrix by using the Schoenberg linear slip theory to obtain the final elastic modulus of "dry" pore rock.

4.2.1. The Schoenberg Linear Slip Theory. The fracture system of the mud shale reservoir of Qingshankou formation (K_2qn) in Sanzhao sag mainly includes interlayer fractures and diagenetic fractures, mainly interlayer fractures. On the basis of the above "dry" pore rock matrix, the elastic model of the "dry" pore rock matrix can be obtained by adding the shale reservoir fractures through the linear sliding theory. Based on the long wave limit theory, Schoenberg proposed the linear sliding theory of fractured media. Different from the Hudson model, Schoenberg believes that the fracture is not ellipsoidal, and the shape of the fracture cannot be accurately described [37]. There is a linear relationship between the displacement of the fracture surface and the stress passing through the fractures, and its linear relationship is given [38].

Table 2: Mineral elastic parameters.

Name	Bulk modulus/GPa	Shear modulus/GPa	Density/(g/cm^3)
Quartz	36.6	45	2.65
Feldspar	37.5	15	2.62
Calcite	76.8	32	2.71
Pyrite	147.4	132.5	4.93
Clay	21	7	2.60
Organic matter	2.9	2.7	1.3
Water	2.23	0	1.04
Oil	0.88	0	0.79

$$\varepsilon_{ij} = \varepsilon_{ijkl}\sigma_{kl} + \frac{1}{2}\int_{Sq} \left([u_i]n_j + [u_j]n_i\right) dS, \tag{13}$$

where u_1, u_2, u_3 denotes, respectively, the displacement in the direction of x_1, x_2, and x_3; S_q represents the surface area of the q fracture in the volume V, n_i represents the ith component of the unit vector perpendicular to the fracture surface. When adding fractures along x_3 to isotropic background media, the medium appears to be the x_3-direction isotropy (HTI), and its elastic matrix is as follows:

$$C^{HTI} = C_b - \begin{bmatrix} \lambda + 2\mu & \lambda\Delta_N & \lambda\Delta_N & 0 & 0 & 0 \\ \lambda\Delta_N & \frac{\lambda^2}{\lambda + 2\mu}\Delta_N & \frac{\lambda^2}{\lambda + 2\mu}\Delta_N & 0 & 0 & 0 \\ \lambda\Delta_N & \frac{\lambda^2}{\lambda + 2\mu}\Delta_N & \frac{\lambda^2}{\lambda + 2\mu}\Delta_N & 0 & 0 & 0 \\ 0 & 0 & 0 & 0 & \mu\Delta_T & 0 \\ 0 & 0 & 0 & 0 & 0 & \mu\Delta_T \end{bmatrix}, \tag{14}$$

where C_b is the elastic matrix of isotropic background medium; N and T, respectively, represent the weakness of fractures, and the expressions are as follows:

$$\Delta_N = \frac{(\lambda + 2\mu)Z_N}{1 + (\lambda + 2\mu)Z_N}, \tag{15}$$

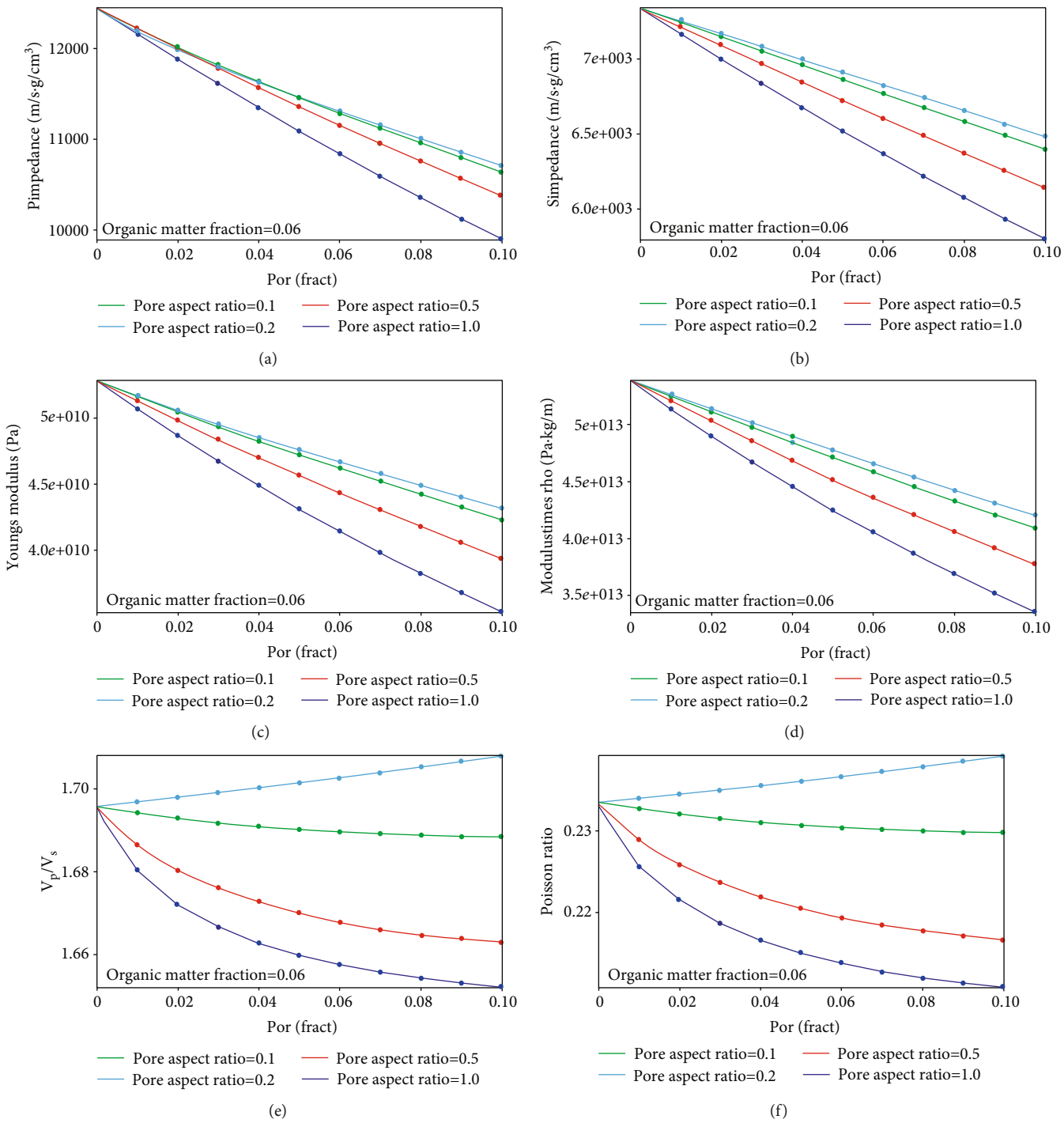

Figure 9: Change of elastic parameters with porosity (the organic volume fraction is 0.06). (a) P-impedance and porosity, (b) S-impedance and porosity, (c) Young's modulus and porosity, (d) Modulus, times Rho, and porosity, (e) Vp/Vs and Porosity, and (f) Poisson's ratio and porosity.

$$\Delta_T = \frac{\mu Z_T}{1 + \mu Z_T}. \tag{16}$$

4.3. Elastic Parameters of Saturated Fluid Rock. The pore fluid of the mud shale reservoir of Qingshankou formation (K_2qn) in Sanzhao sag contains oil and water. Therefore, the wood formula [39] can be applied to mix the pore fluid (oil and water) to obtain the bulk modulus of the mixed fluid. The Gassmann equation [40] is based on the assumption of isotropy and cannot meet the needs of the physical modeling of anisotropic shale rocks. Brown and Korringa derived the Gassmann equation in the anisotropic form [41] and the Brown-Korringa formula can be applied to describe the theoretical relationship of equivalent modulus

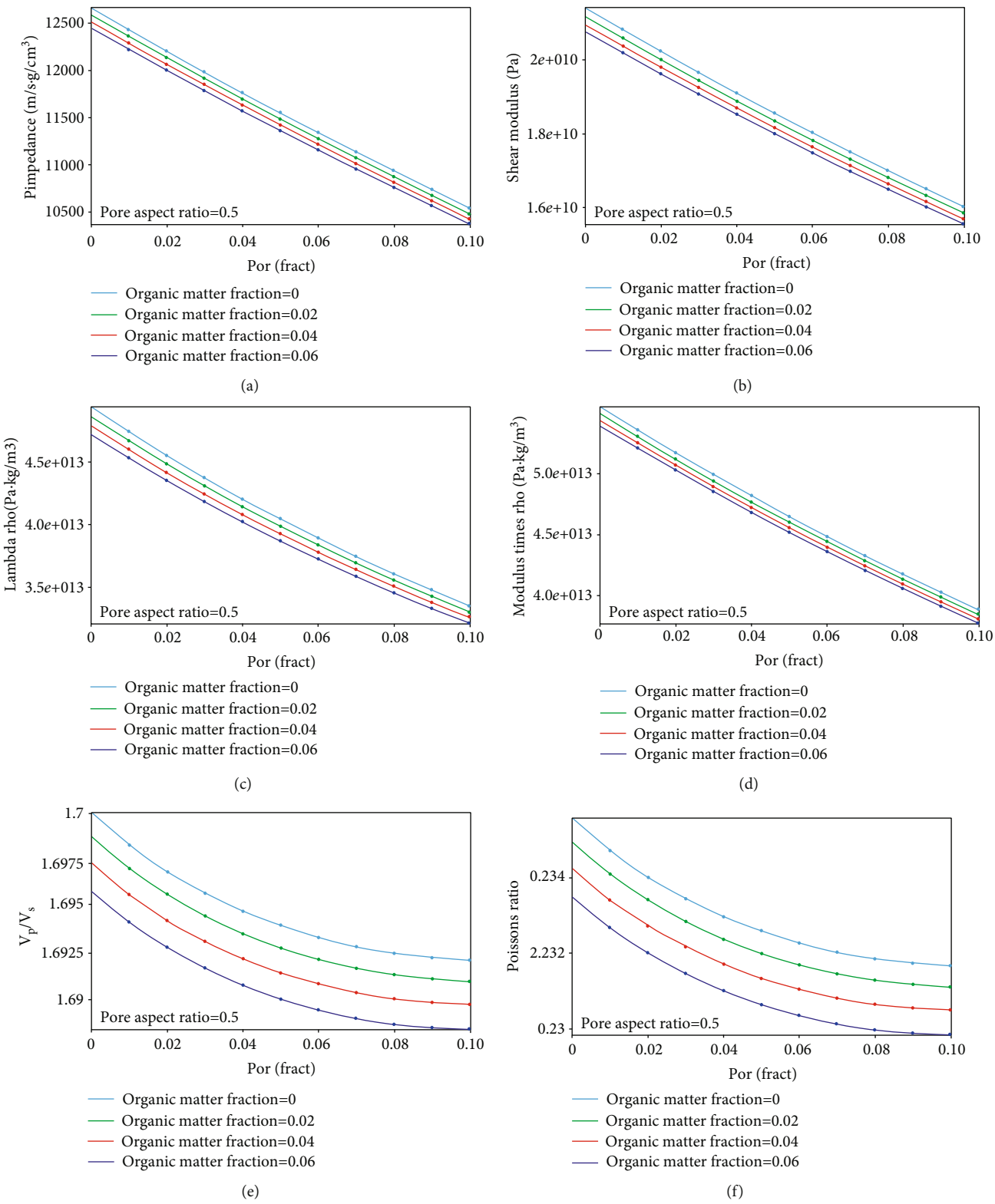

Figure 10: Change of elastic parameters with porosity (porosity aspect ratio is 0.5). (a) P-impedance and porosity, (b) S-impedance and porosity, (c) lambda rho and porosity, (d) Modulus times rho and porosity, (e) Vp/Vs and porosity, and (f) Poisson's ratio and porosity.

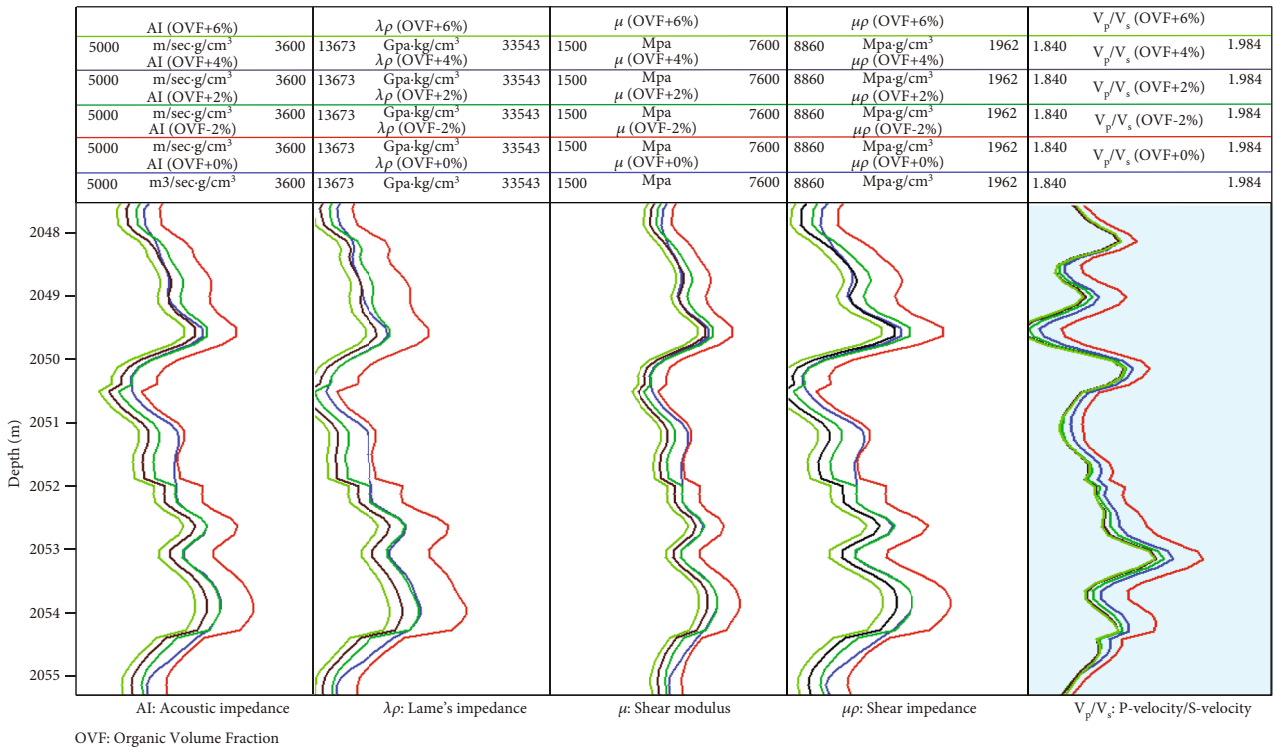

Figure 11: Elastic parameter curve of different organic volume fractions.

of anisotropic rock matrix when it is saturated with fluid. The specific formula is as follows:

$$S_{\mathrm{ijkl}}^{\mathrm{eff}} = S_{\mathrm{ijkl}}^{\mathrm{dry}} - \frac{\left(S_{\mathrm{ijmn}}^{\mathrm{dry}} - S_{\mathrm{ijmn}}^{\mathrm{gr}}\right)\left(S_{\mathrm{klpq}}^{\mathrm{dry}} - S_{\mathrm{klpq}}^{\mathrm{gr}}\right)}{\left[\varphi\left(S^{\mathrm{toc}} - S^{\varphi}\right) + \left(S^{\mathrm{dry}} - S^{\mathrm{gr}}\right)\right]_{\mathrm{nmpq}}}, \tag{17}$$

where φ is the volume fraction of organic matter, $S_{\mathrm{ijkl}}^{\mathrm{gr}}$, $S_{\mathrm{ijkl}}^{\mathrm{dry}}$, and $S_{\mathrm{ijkl}}^{\mathrm{eff}}$ refer to the granular minerals, the "dry" matrix, and the fourth-order flexibility tensor of the final equivalent result, respectively. S^{φ} and S^{toc} refer to the flexibility tensor of inclusion space and organic matter, respectively.

5. Rock Physical Characteristics

5.1. Influencing Factors of Reservoir Parameters. Based on the established physical model of shale rock with complex pore structure, the influence of three factors, i.e., organic volume fraction, matrix porosity, and pore aspect ratio, on rock elastic parameters, is systematically analyzed, which provides a theoretical basis for the establishment of physical cross-plot template of shale rock. Modulus parameters of key minerals and fluids were obtained through the core test of Qingshankou formation (K_2qn) in Sanzhao sag (Table 2).

5.1.1. Effect of Porosity and Pore Aspect Ratio. Figure 9 reveals the changes of elastic parameters with matrix porosity and pore aspect ratio. The range of matrix porosity is 0-0.1, the range of pore aspect ratio is 0.1-1.0, and the organic volume fraction is 0.06. It can be seen that with the increase of matrix porosity, all elastic parameters show

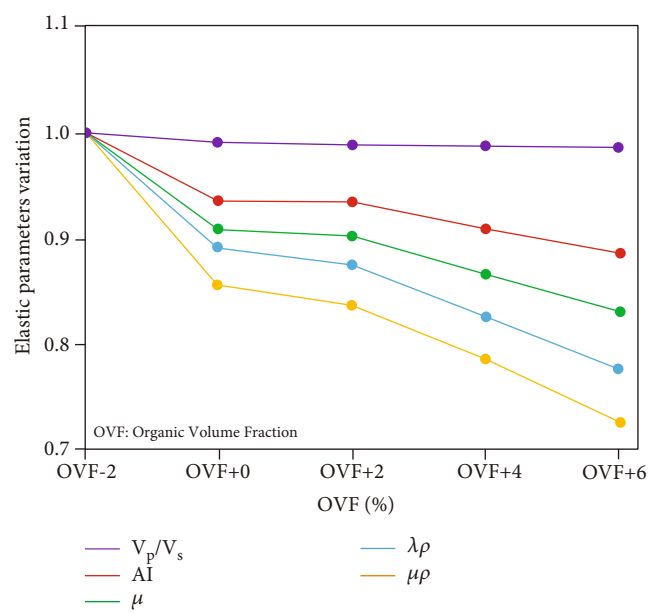

Figure 12: Effect of different organic volume fractions on elastic parameters.

a decreasing trend, but the changing trend of Poisson's ratio and Vp/Vs is reversed when the aspect ratio is between 0.8-1, that is, it increases with the increase of matrix porosity. With the increase of the pore aspect ratio, all elastic parameters change obviously. With the increase of pore aspect ratio, except Poisson's ratio and Vp/Vs, other elastic parameters show an increasing trend. The larger the matrix

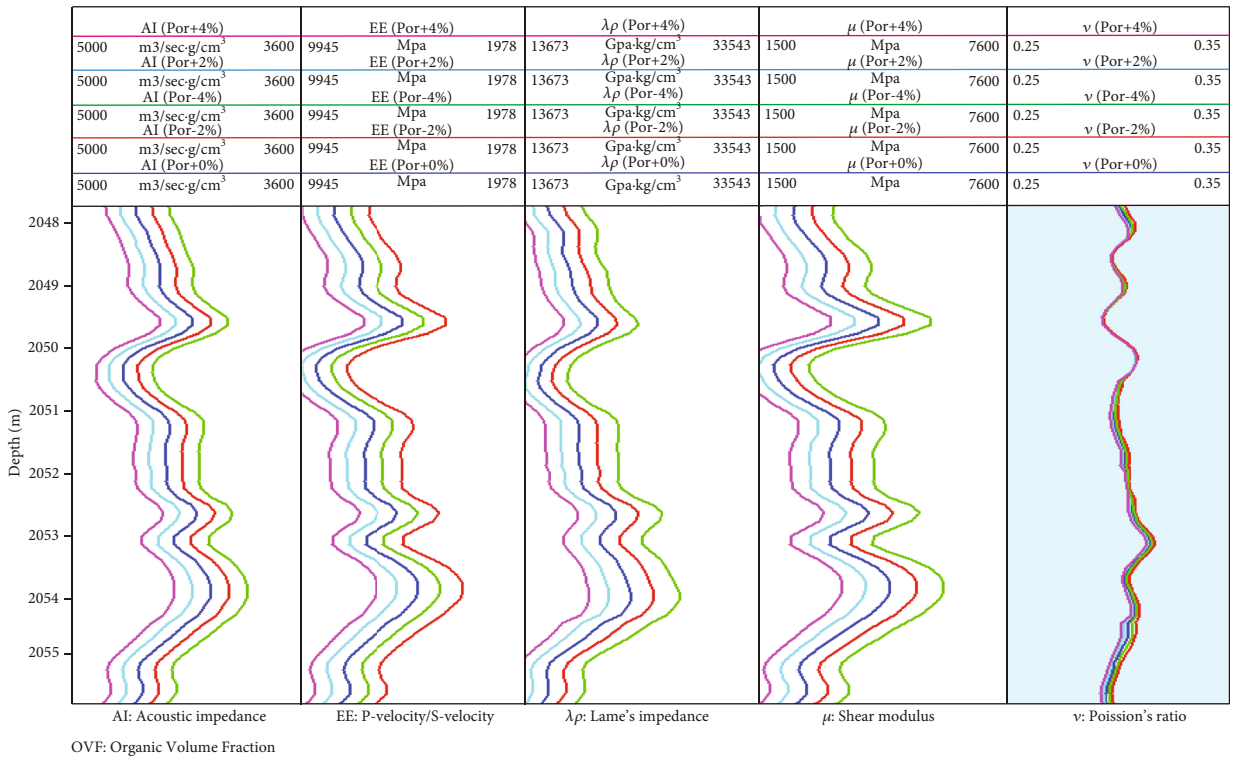

Figure 13: Elastic parameter curve of variable porosity.

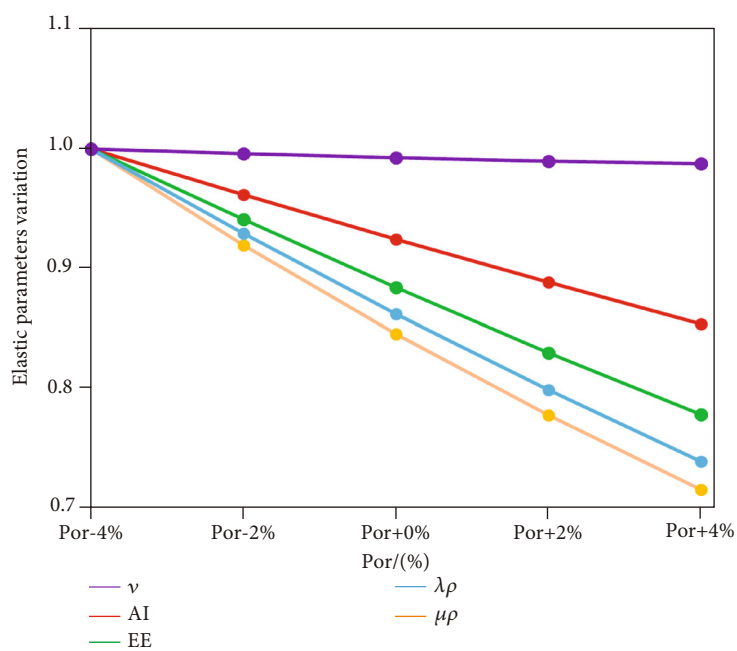

Figure 14: Effect of porosity on elastic parameters.

porosity is, the more obvious the change of elastic parameters is with the change of pore aspect ratio, and the changes of Vp/Vs and Poisson's ratio are more obvious.

5.1.2. Effect of the Organic Volume Fraction and Porosity. Figure 10 reveals the changes of elastic parameters with matrix porosity and the organic volume fraction. The range of matrix porosity is 0-0.1, the organic volume fraction is 0-0.06, and the pore aspect ratio is 0.5. With the increase of the organic volume fraction, all elastic parameters except shear modulus (μ) show an increasing trend. In comparison, the changing trend of P-wave impedance(AI),

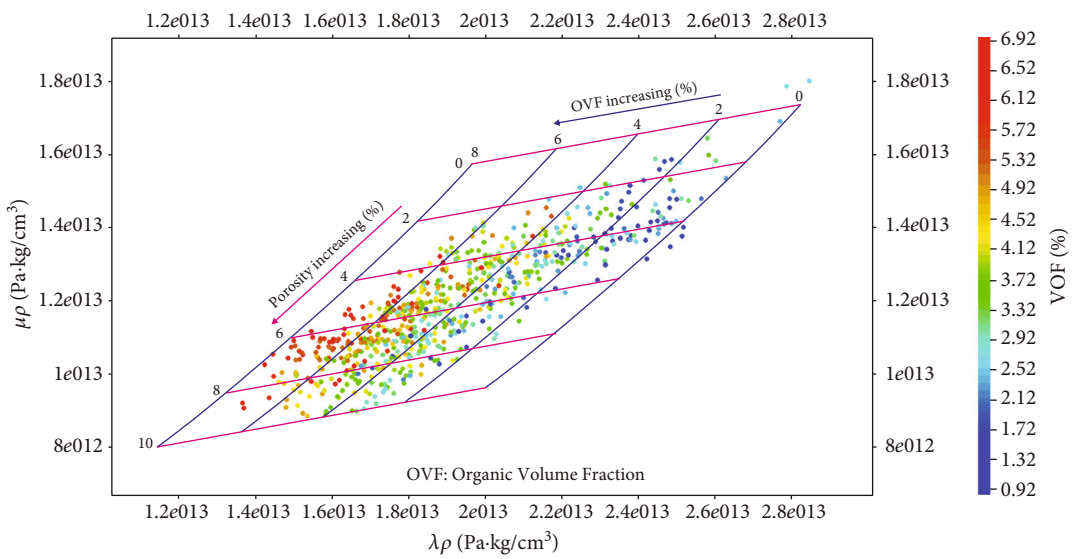

Figure 15: Petrophysical template of the organic volume fraction and porosity.

shear modulus (μ), $\lambda\rho$, and $\mu\rho$ is approximately linear. For the elastic parameters of Vp/Vs and Poisson's ratio, when the porosity is less than 5%, the decreasing range is more than 5%, and with the increase of the organic volume fraction, the elastic parameters of Vp/Vs and Poisson's ratio change most obviously.

6. Rock Physics Template

The organic volume fraction and total porosity play an important role in the process of shale oil reservoir evaluation and are the key parameters of shale oil "sweet spot" evaluation. The pore volume determines the reservoir space of shale oil. The organic volume fraction is the main index to evaluate the organic matter abundance and hydrocarbon generation capacity of shale, which affects the oil generation potential and storage capacity of shale and further determines the oil content and productivity of shale reservoir. It is necessary to carry out forward modeling of the organic volume fraction and total porosity, to clarify its geophysical characteristics, and to provide a basis for subsequent "sweet spot" prediction. Based on the shale rock physical model, taking the 2048-2055 m sweet layer of SYY3 as the research object, on the basis of the original organic matter volume fraction and porosity, increase and decrease the organic volume fraction (OVF) and porosity fraction, simulate the seismic response under the conditions of different organic matter volume fraction and porosity fraction, and further analyze the elastic parameters and characteristic change laws. The sensitive parameters that can identify organic matter and pores are selected, using the sensitive parameters to construct the rock physical template of the shale oil reservoir.

Figure 11 is an elastic parameter forward modeling curve under the condition of varying organic volume fractions. The curve from left to right is the P-wave impedance (AI), $\lambda\rho$, shear modulus (μ), $\mu\rho$, and Vp/Vs; the blue in each track represents the original curve (OVF + 0%), the red represents

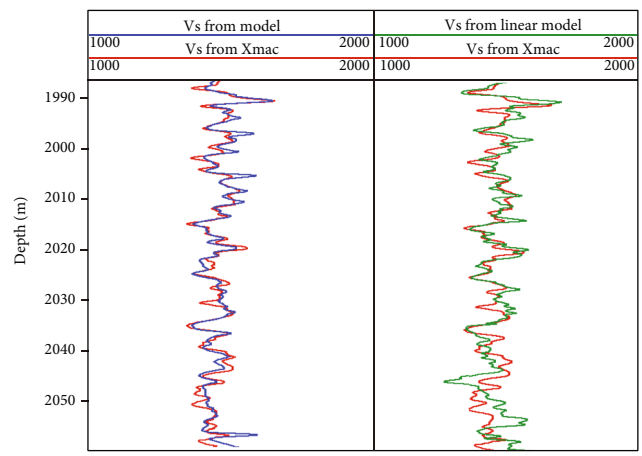

Figure 16: Vs prediction comparison between petrophysical model and Vp/Vs linear regression formula.

the forward curve with the organic volume fraction reduced by 2% (OVF − 2%), the dark green represents the forward curve with the organic volume fraction increased by 2% (OVF + 2%), the magenta represents the forward curve with the organic volume fraction increased by 4% (OVF + 4%), and the light green represents the forward curve with the organic volume fraction increased by 6% (OVF + 6%). In Figure 11, when the organic volume fraction decreases by 2%, all elastic parameters increase, and when the organic volume fraction gradually increases by 2%, 4%, and 6%, all elastic parameters show a decreasing trend. In order to further quantify the sensitive elastic parameters of the organic volume fraction, the relative change of each elastic parameter with the change of the organic volume fraction (Figure 12) is established. It can be seen that the order of sensitive parameters for identifying organic matter are $\lambda\rho$, $\mu\rho$, shear modulus (μ), P-wave impedance(AI), and Vp/Vs.

Figure 13 is the elastic parameter forward modeling curve under the condition of variable porosity. From the left

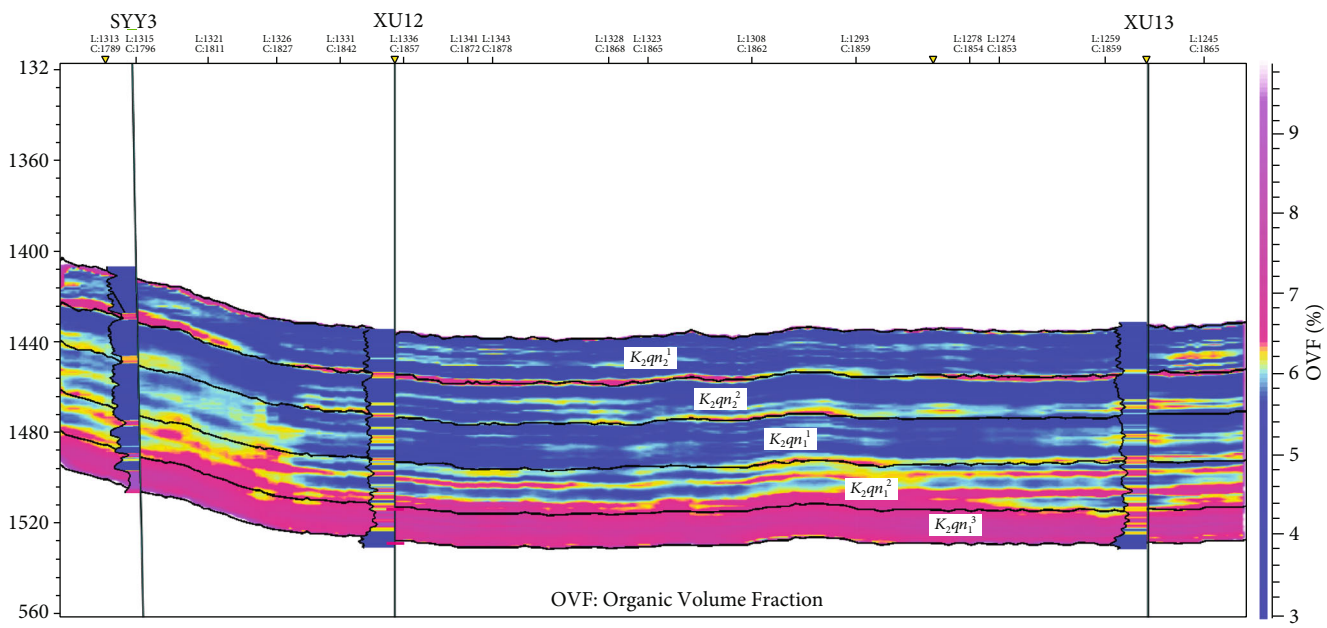

Figure 17: The organic volume fraction cross-section of SYY3, XU12, and XU13.

to right, the curves of the track are the P-wave impedance (AI), Young's modulus (E), $\lambda\rho$, $\mu\rho$, and shear modulus (μ). The blue curve in each track represents the original curve (Por + 0%), the red curve represents the forward curve with porosity reduced by 2% (Por − 2%), the dark green curve represents the forward curve with porosity reduced by 4% (Por − 4%), the magenta curve represents the forward curve with porosity increased by 2% (Por + 2%), and the light green curve represents the forward curve with porosity increased by 4% (Por + 4%). It can be seen from the figure that with the increase of porosity, all elastic parameters show a decreasing trend. In order to further quantify the sensitive elastic parameters of the organic volume fraction, the relative change curve of each elastic parameter with porosity change is constructed (Figure 14). It can be seen that the order of sensitive parameters for identifying porosity is $\mu\rho$, $\lambda\rho$, P-wave impedance (AI), Young's modulus (E), and shear modulus (μ).

Through comparison and optimization, $\lambda\rho$ and $\mu\rho$ are finally determined as the sensitive parameters for identifying organic matter and pores. As the two parameters' changing directions are unique and the correlation is weak, which can be applied to the construction of a shale rock physical template. In the construction process, based on the physical model of shale rock and taking $\lambda\rho$ and $\mu\rho$ as the horizontal and vertical coordinates, the water saturation curves under different mineral component contents are obtained by using the water saturation model of mineral components; the template is corrected with the core test data. The template is corrected with the core test, and a shale rock physical cross-plot template is established in which the matrix minerals are quartz, feldspar, calcite, pyrite, and clay; the organic volume fraction is 0%, 2%, 4%, 6%, and 8%, the total porosity is 0-10%, and the pore fluid is water and oil. The applicability of the petrophysical template is verified by the data of shale wells in the Qingshankou formation (K_2qn) of Sanzhao sag in the north of Songliao basin. The verification results are shown in Figure 15. The color in the figure indicates the organic volume fraction. It can be seen that the actual data point positions of different the organic volumes fraction and different porosity are also basically consistent with the results of the petrophysical template, which can effectively distinguish different the organic volumes fraction and different porosity, and can be used as the basis for the evaluation of the shale reservoir of Qingshankou formation (K_2qn) in Songliao basin and the identification of "sweet spot".

7. Vs Prediction

The Vs of SYY3 well in Qingshankou formation (K_2qn) of Sanzhao sag in the north of Songliao basin is predicted by using the anisotropic shale petrophysical model. The volume fraction of various mineral components, organic matter, matrix porosity, and saturation information in the well are obtained through logging interpretation and core testing correction. The pore aspect ratio is obtained based on the 3D image statistics of digital core sample nano CT scanning, and the pore aspect ratio is 0.55.

Figure 16 shows the comparison between the Vs predicted and that measured by dipole source logging. It can be seen that compared with the Vs obtained by using the Vp linear regression formula, the Vs obtained based on the petrophysical model is more accurate and is basically consistent with the measured Vs velocity, with a good coincidence and a relative error of less than 5%, ensuring the reliability and applicability of the shale rock physical model proposed in this paper.

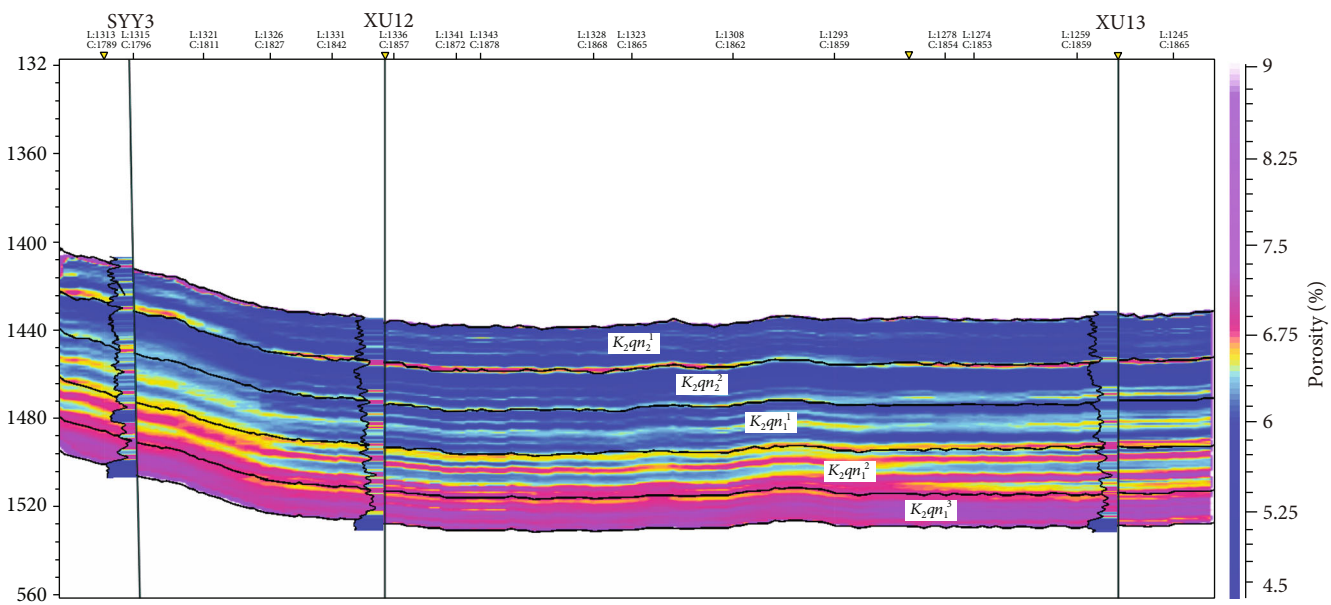

Figure 18: Porosity cross-section of SYY3, XU12, and XU13.

8. Application of "Sweet Spot" Prediction

Taking the middle part of Sanzhao sag as the research object, the key parameters (the organic volume fraction and porosity) of shale oil "sweet spot" are predicted by using 3D seismic data. The study area is located in the middle of Sanzhao sag, with a relatively stable structure. There are few drilling wells in the work area. The aspect ratio of seismic data is 0.62, and the offset is 210-3500 m. The signal-to-noise ratio of seismic data is high, providing a basis for the prediction of shale oil seismic "sweet spot." Prestack elastic parameter inversion is the key to predict shale oil's "sweet spot," and its inversion results are greatly affected by the quality of prestack gathers. Before prestack inversion, a series of optimization processes including super gather noise removal, anisotropy correction flattening, and residual energy compensation should be performed to obtain high-quality prestack gathers, and $\lambda\rho$ and $\mu\rho$ could be calculated as well. According to the petrophysical analysis results, the well location (the organic volume fraction, porosity) is taken as the main variable, $\lambda\rho$ and $\mu\rho$ are taken as the covariate, and the distribution of the organic volume fraction and porosity is predicted by extrapolation between wells under seismic constraints (Figure 17, Figure 18). It can be seen from the figures that from bottom to top, the organic volume fraction and porosity show a gradually decreasing trend, which is consistent with their changing trends, that is, with the increase of the organic volume fraction, the porosity gradually increases, which reflects that nanopores are widely developed in organic-rich shale during the deposition process with the increase of evolution degree, and they are important storage spaces for shale oil. The organic volume fraction and porosity of the $K_2qn_1^3$ are the highest, with the organic volume fraction of 9.1% and porosity of 9.5%, showing a relatively continuous distribution horizontally. The $K_2qn_1^2$ formation also develops shale rich in organic matter, but compared with the $K_2qn_1^3$ formation, the organic volume fraction and porosity are discontinuous vertically, and there is an interlayer with a thickness of about 8 m. The SYY3 well-obtained shale industrial oil flow by fracturing in the $K_2qn_1^3$ oil formation.

9. Conclusions

(1) An anisotropy petrophysical model with complex pore structure suitable for organic shale is proposed by comprehensively using the Voigt-Reuss-Hill average model; the anisotropy SCA+DEM model, the layering of clay and kerogen, is simulated by using the V-R-H average and bond transform to achieve the simulation of shale anisotropy

(2) The effects of organic volume fraction, porosity, and pore aspect ratio on rock elastic parameters are systematically analyzed by using the shale rock physical model. With the increase of matrix porosity, all elastic parameters show a decreasing trend, but when the aspect ratio is between 0.8 and 1, the changing trend of the Poisson's ratio and Vp/Vs is reversed, that is, those increases with the increase of matrix porosity. With the increase of pore aspect ratio, all other elastic parameters except Poisson's ratio and Vp/Vs show an increasing trend, and when changing the pore aspect ratio, the larger the matrix porosity, the more obvious the changes of elastic parameters, and the changes of Vp/Vs and Poisson's ratio are the most obvious. With the increase of organic volume fraction, except shear modulus (μ), other elastic parameters show an increasing trend. In comparison, the changing trend of P-wave impedance (AI), shear modulus (μ), $\lambda\rho$, and $\mu\rho$ is approximately

linear, which provides a theoretical basis for the construction of shale rock physical cross-plot template

(3) Based on the shale rock physical model and the analysis of elastic parameter influencing factors, the elastic parameters $\lambda\rho$ and $\mu\rho$ sensitive to organic matter and pores are optimized, and the shale rock physical cross-plot template that can distinguish different organic volume fractions and porosity is constructed

(4) The application shows that the predicted Vs based on the proposed model is in good agreement with the Vs derived from dipole source logging. Through prestack elastic parameter inversion, the "sweet spot" characteristics are well described, which provides an important support for the deployment of shale oil wells in Sanzhao sag

Data Availability

The raw data supporting the conclusions of this article will be made available by the authors, without undue reservation.

Conflicts of Interest

Author Ang Li is employed by the Shenyang Centre of Geological Survey, China Geological Survey, Shenyang, Liaoning, China. The remaining authors declare that the research was conducted in the absence of any commercial or financial relationships that could be construed as a potential conflict of interest.

Authors' Contributions

The first author Ang Li is responsible for the idea and writing of this article, and the coauthors LYZ, GJY, SCL, FX, YLY, YMH, BL, and LSL are responsible for the experimental part.

Acknowledgments

The support of the National Natural Science Foundation of China Youth Fund Project (41804138 and 42204113) is appreciated.

References

[1] I. J. Anderson, J. S. Ma, X. Y. Wu, and D. Stow, "Determining reservoir intervals in the Bowland shale using petrophysics and rock physics models," *Geophysical Journal International*, vol. 228, no. 1, pp. 39–65, 2021.

[2] A. Li, L. Y. Zhang, J. G. Yang, and Y. M. Huang, "Seismic method for shale oil sweet spot prediction in Qingshankou formation of Sanzhao sag, Songliao basin," *Geology and Resources*, vol. 30, no. 3, pp. 366–376, 2021.

[3] Q. Zhou, Z. Jin, G. Yang, N. Dong, and Z. Shang, "Shale oil exploration and production in the US: status and outlook," *Oil &. Gas Geology*, vol. 40, no. 3, pp. 469–477, 2019.

[4] Q. Ren and K. T. Spikes, "Modeling the effects of microscale fabric complexity on the anisotropy of the Eagle Ford shale," *Interpretation*, vol. 4, no. 2, pp. SE17–SE29, 2016.

[5] P. Avseth, "Geological processes and rock physics signatures of upper Jurassic organic-rich shales, Norwegian shelf," in *76th EAGE Conference and Exhibition*, Amsterdam RAI, The Netherlands, 2014.

[6] C. M. Sayers and S. Dasgupta, "A predictive anisotropic rock-physics model for estimating elastic rock properties of unconventional shale reservoirs," *The Leading Edge*, vol. 38, no. 5, pp. 358–365, 2019.

[7] C. H. Sondergeld, C. S. Rai, R. W. Margesson, and K. J. Whidden, "Ultrasonic measurement of anisotropy on the Kimmeridge shale," in *SEG Technical Program Expanded Abstracts 2000*, pp. 1858–1861, Calgary, Canada, 2000.

[8] C. H. Sondergeld and C. S. Rai, "Elastic anisotropy of shales," *The Leading Edge*, vol. 30, no. 3, pp. 324–331, 2011.

[9] C. M. Sayers, "Seismic anisotropy of shales," *Geophysical Prospecting*, vol. 53, no. 5, pp. 667–676, 2005.

[10] J. E. Johnston and N. I. Christensen, "Seismic anisotropy of shales," *Journal of Geophysical Research - Solid Earth*, vol. 100, no. B4, pp. 5991–6003, 1995.

[11] G. Mavko, T. Mukerji, and J. Dvorkin, *Rock Physics Handbook. Tools for Seismic Analysis of Porous Media*, Cambridge University Press, New York, 2011.

[12] B. E. Hornby, L. M. Schwartz, and J. A. Hudson, "Anisotropic effective-medium modeling of the elastic properties of shales," *Geophysics*, vol. 59, no. 10, pp. 1570–1583, 1994.

[13] G. E. Backus, "Long-wave elastic anisotropy produced by horizontal layering," *Journal of Geophysical Research*, vol. 67, no. 11, pp. 4427–4440, 1962.

[14] L. Vernik and C. Landis, "Elastic anisotropy of source rocks: implications for hydrocarbon generation and primary migration," *AAPG Bulletin*, vol. 80, no. 4, pp. 531–544, 1996.

[15] C. M. Sayers, "The effect of kerogen on the elastic anisotropy of organic-rich shales," *Geophysics*, vol. 78, no. 2, pp. D65–D74, 2013.

[16] Z. Guo and X. Y. Li, "Rock physics model-based prediction of shear wave velocity in the Barnett shale formation," *Journal of Geophysics and Engineering*, vol. 12, no. 3, pp. 527–534, 2015.

[17] K. Bandyopadhyay, *Seismic Anisotropy: Geological Causes and Its Implications to Reservoir Geophysics, [Ph.D. thesis]*, Stanford University, San Francisco, 2009.

[18] X. Wu, R. Uden, and M. Chapman, "Shale anisotropic elastic modelling and seismic reflections," *Journal of Seismic Exploration*, vol. 25, no. 6, pp. 527–542, 2016.

[19] A. Drage, M. Jakobsen, and T. A. Johansen, "Rock physics modelling of shale diagenesis," *Petroleum Geoscience*, vol. 12, no. 1, pp. 49–57, 2006.

[20] Q. Hu, X. H. Chen, and Y. Guo, "A rock physics model of kerogen inclusions in shale," in *SEG Technical Program Expanded Abstracts 2013*, Houston, USA, 2013.

[21] R. N. Vasin, H. R. Wenk, W. Kanitpanyacharoen, S. Matthies, and R. Wirth, "Elastic anisotropy modeling of Kimmeridge shale," *Journal of Geophysical Research: Solid Earth*, vol. 118, no. 8, pp. 3931–3956, 2013.

[22] J. C. Gui, J. C. Guo, Y. Sang, Y. X. Chen, T. S. Ma, and P. G. Ranjith, "Evaluation on the anisotropic brittleness index of shale rock using geophysical logging," *Petroleum*, pp. 2405–6561, 2022.

[23] R. M. Pollastro, D. M. Jarvie, R. J. Hill, and C. W. Adams, "Geologic framework of the Mississippian Barnett shale, Barnett-Paleozoic total petroleum system, bend arch–Fort Worth Basin, Texas," *AAPG Bulletin*, vol. 91, no. 4, pp. 405–436, 2007.

[24] Q. Wang, Q. Hu, X. Ning, J. Ilavsky, I. Kuzmenko, and T. Tom, "Spatial heterogeneity analyses of pore structure and mineral composition of Barnett shale using X-ray scattering techniques," *Marine and Petroleum Geology*, vol. 134, article 105354, 2021.

[25] Q. T. Wang, T. L. Wang, W. P. Liu et al., "Relationships among composition, porosity and permeability of Longmaxi shale reservoir in the Weiyuan block, Sichuan Basin, China," *Marine and Petroleum Geology*, vol. 102, pp. 33–47, 2019.

[26] A. B. Andhumoudine, X. Nie, Q. B. Zhou et al., "Investigation of coal elastic properties based on digital core technology and finite element method," *Advances in Geo-Energy Research*, vol. 5, no. 1, pp. 53–63, 2021.

[27] T. S. Ma and P. Chen, "Study of meso-damage characteristics of shale hydration based on CT scanning technology," *Petroleum Exploration and Development*, vol. 41, no. 2, pp. 249–256, 2014.

[28] T. S. Ma, C. H. Yang, P. Chen, X. D. Wang, and Y. T. Guo, "On the damage constitutive model for hydrated shale using CT scanning technology," *Journal of Natural Gas Science and Engineering*, vol. 28, pp. 204–214, 2016.

[29] Y. Wei, X. Nie, L. D. Jin, C. Zhang, C. M. Zhang, and Z. S. Zhang, "Investigation of sensitivity of shale elastic properties to rock components based on a digital core technology and finite element method," *Arabian Journal of Geosciences*, vol. 11, no. 10, 2018.

[30] B. K. Li, X. Nie, J. C. Cai, X. Zhou, C. Wang, and D. Han, "U-net model for multi-component digital rock modeling of shales based on CT and QEMSCAN images," *Journal of Petroleum Science and Engineering*, vol. 216, article 110734, 2022.

[31] W. Voigt, *Lehrbuch der Kirstallphysik: Teubner-Leipzig*, Macmillan, New York, 1928.

[32] B. Budiansky, "On the elastic moduli of some heterogeneous materials," *Journal of the Mechanics and Physics of Solids*, vol. 13, no. 4, pp. 223–227, 1965.

[33] R. Hill, "A self-consistent mechanics of composite materials," *Journal of the Mechanics and Physics of Solids*, vol. 13, no. 4, pp. 213–222, 1965.

[34] A. N. Norris, P. Sheng, and A. J. Callegari, "Effective medium theories for two phase dielectric media," *Applied Physics*, vol. 57, no. 6, pp. 1990–1996, 1985.

[35] R. W. Zimmerman, *Compressibility of Sandstones*, Elsevier, New York, 1991.

[36] H. Z. Yuan, *Study of Anisotropic Rock Physics Model and Application*, China University of Petroleum, 2007.

[37] X. Y. Yin and X. W. Maz, "Review of fracture prediction driven by the seismic rock physics theory (I): effective anisotropic seismic rock physics theory," *Geophysical Prospecting for Petroleum*, vol. 61, no. 2, pp. 183–204, 2022.

[38] M. Schoenberg and C. M. Sayers, "Seismic anisotropy of fractured rock," *Geophysics*, vol. 60, no. 1, pp. 204–211, 1995.

[39] A. W. Wood, *A Textbook of Sound*, The MacMillan Co, New York, 1955.

[40] F. Gassmann, "Elastic waves through. A packing of spheres," *Geophysics*, vol. 16, no. 4, pp. 673–685, 1951.

[41] R. J. S. Brown and J. Korringa, "On the dependence of the elastic properties of a porous rock on the compressibility of the pore fluid," *Geophysics*, vol. 40, no. 4, pp. 608–616, 1975.